S. Vasista, A. De Gaspari, S. Ricci, J. Riemenschneider, H.P. Monner, B. van de Kamp
Compliant Structures-Based Wing and Wingtip Morphing Devices
Aircraft Engineering and Aerospace Technology, Vol. 88, N. 2, 2016, p. 311-330
doi:10.1108/AEAT-02-2015-0067

Compliant Structures-Based Wing and Wingtip Morphing Devices

Contact Information:

1. Srinivas Vasista

Alexander von Humboldt Postdoctoral Research Fellow

Department of Adaptronics, Institute of Composite Structures and Adaptive Systems

German Aerospace Center (DLR)

Lilienthalplatz 7, Braunschweig 38108, Germany

srinivas.vasista@dlr.de

+49 (531) 295-3247

2. Alessandro De Gaspari

Post-doctoral Researcher

Department of Aerospace Science and Technology

Politecnico di Milano

Via La Masa 34, 20156 Milano, Italy

alessandro.degaspari@polimi.it

3. Sergio Ricci

Associate Professor

Department of Aerospace Science and Technology

Politecnico di Milano

Via La Masa 34, 20156 Milano, Italy

sergio.ricci@polimi.it

4. Johannes Riemenschneider

Deputy Head of Department

Department of Adaptronics, Institute of Composite Structures and Adaptive Systems

German Aerospace Center (DLR)

Lilienthalplatz 7, Braunschweig 38108, Germany

Johannes.riemenschneider@dlr.de

+49 (531) 295-2388

5. Hans Peter Monner

Head of Department

Department of Adaptronics, Institute of Composite Structures and Adaptive Systems

German Aerospace Center (DLR)

Lilienthalplatz 7, Braunschweig 38108, Germany

hans.monner@dlr.de

+49 (531) 295-2314

6. Bram van de Kamp

Research Engineer

Department of Adaptronics, Institute of Composite Structures and Adaptive Systems

German Aerospace Center (DLR)

Lilienthalplatz 7, Braunschweig 38108, Germany

bram.vandekamp@dlr.de

+49 (531) 295-2354

Compliant Structures-Based Wing and Wingtip Morphing Devices

Abstract

Purpose – The aim of this paper is to provide an overview of the design and experimental work of compliant wing and wingtip morphing devices conducted within the EU FP7 project NOVEMOR and to demonstrate that the optimization tools developed can be used to synthesise compliant morphing devices.

Design/methodology/approach – The compliant morphing devices were "designed-through-optimization", with the optimization algorithms including Simplex optimization for composite compliant skin design, aerodynamic shape optimization able to take into account the structural behaviour of the morphing skin, continuum-based and load path representation topology optimization methods and multi—objective optimization coupled with genetic algorithm for compliant internal substructure design. Low speed subsonic wind tunnel testing was performed as an effective means of demonstrating proof-of-concept.

Findings – It was found that the optimization tools could be successfully implemented in the manufacture and testing stage. Preliminary insight into the performance of the compliant structure has been made during the first wind tunnel tests.

Practical implications – The tools in this work further the development of morphing structures, which when implemented in aircraft have potential implications to environmental friendlier aircraft.

Originality/value – The key innovations in this paper include the development of a composite skin optimization tool for the design of highly 3D morphing wings and its ensuing manufacture process; the development of a continuum-based topology optimization tool for shape control design of compliant mechanisms considering the stiffness and displacement functions, the use of a superelastic material for the compliant mechanism; wind tunnel validation of morphing wing devices based on compliant structure technology.

Keywords Morphing structures; compliant mechanisms; topology optimization, genetic algorithm, multi—objective optimization.

Paper type Research paper.

Introduction

The European Union has identified under the 7th Framework Programme that there is need for the development of integrated, safer, greener and smarter pan-European sustainable transport systems, specifically emphasising the reduction of aircraft emissions and environmentally friendlier aviation (CORDIS, 2012). Reports and schemes such as the VISION2020 (ACARE, 2001) and Flightpath2050 (European Commission, 2011) call for ambitious targets for the reduction of emissions, such as reducing CO_2 emissions per passenger kilometre by 50% by 2020 and 75% by 2050, NOx emissions by 80% by 2020 and 90% by 2050, and perceived noise by 50% by 2020 and 65% by 2050, in comparison to the capabilities of new aircraft in 2000. Morphing technology is a solution with high potential to help meet such ambitious targets (Stanewsky, 2000) and while there are many challenges yet to overcome, steps are being made towards the realization of morphing devices and implementation in aircraft (Norris, 2015). The main rationale behind using morphing devices is that the aircraft can adapt its shape to best suit the prevailing conditions, thereby operating at a higher efficiency over the full range of flight conditions in its mission profile. Morphing in a smoothly varying, gapless, continuous manner, as a particular type of morphing and more than just changing shape in general, has added benefits. With the absence of gaps and sharp changes to the aerodynamic surface, the resulting flow is more laminar and less noise will be emitted (Kintscher *et al*., 2011). In light of the potential benefits that smoothly varying continuous morphing devices can afford, significant efforts are being made by the research community and industry to successfully design and implement such structures in aircraft. There are a number of review papers on the field of morphing structures research (Weisshaar, 2013; Vasista *et al*., 2012; Barbarino *et al*., 2011; Sofla *et al*., 2010; Thill *et al*., 2008), indicating the status, benefits and outlook of morphing technology and the reader is referred to these works for further background and information.

The European FP7 project NOVEMOR (“Novel Air Vehicle Configurations: from Fluttering Wings to Morphing Flight”) comprises many aspects of morphing aircraft structures research (Suleman *et al*., 2014), including the design and testing of morphing devices for a regional jetliner wing. The reference geometry, provided by project partner Embraer, is shown in Figure 1 and features compliant morphing devices throughout the wing and wingtip. The anticipated aircraft performance benefits of such technology include reduced drag and lift-distribution tailoring through wing camber adjustments over the total flight mission, and aeroelastic benefits such as the improvement of the loss of aileron efficiency with increasing dynamic pressure. Compliant structures, or compliant mechanisms, have advantages over their counterpart conventional rigid-link mechanisms, such as the elimination of backlash, reduced assembly complexities, time and costs, and potentially lower weight. (Lu & Kota, 2005) This reference wing was subdivided into the wing and wingtip regions; the structural design of the droop-nose morphing wingtip was conducted by the German Aerospace Center (DLR) whilst the structural design of morphing leading and trailing edge devices in the wing was performed by the Politecnico di Milano

(POLIMI). In this manner, various design tools and methodologies could be explored and assessed and applied to real aircraft geometries. This paper collates and describes the different design methodologies and tools used by the DLR and POLIMI and the results associated with each. Fundamental to the project was the assessment of the structural performance of the morphing devices under aerodynamic loads, and the manufacture was conducted with wind tunnel testing as a mandatory task in mind. The DLR morphing wingtip is first presented, which features a flexible optimized composite skin supported by internal superelastic nickel-titanium and aluminium alloy compliant structures designed through continuum-based topology optimization. The designs of the POLIMI morphing wing devices via a parametric framework including the codes PHORMA and SPHERA, are subsequently described. The test setup of a scaled prototype fabricated using 3D printing technologies is shown thereafter.

Figure 1 NOVEMOR aircraft geometry with wing and wingtip regions defined.

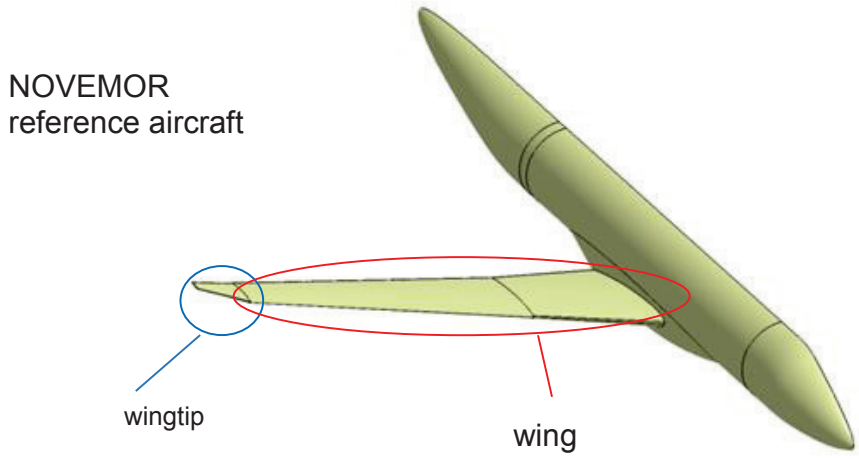

DLR Droop-Nose Morphing Wingtip

Design Chain

The geometry of the wingtip is shown in Figure 2 and is characterized by a sweep angle (~ 35°), taper ratio (~ 0.5) in both chord and thickness direction, dihedral angle (~ 14°), curvature in multiple directions and a droop-nose target deflection (~ 2°). The span length is 1488 mm and the DLR is currently constructing a full-scale prototype for wind tunnel testing in collaboration with the University of Bristol, though with 100 mm trimmed at both the inboard and outboard stations due to size constraints of the wind tunnel. The highly 3D nature of the geometry poses challenges to the design of the morphing device and the optimization tools developed in this work are new developments aimed at handling these geometrical challenges.

The structural design of the DLR NOVEMOR droop-nose morphing wingtip involves a number of processes and follows a design chain as established by Kintscher *et al*. (2011), Rudenko *et al*. (2014) and Radestock *et al*. (2014). This design chain is shown in Figure 3 and the underlying rationale of this approach stems from the requirement of 1. a skin with tailored stiffness and flexibility such that it is able to morph its shape yet also carry flight loads and 2. an internal compliant mechanism which can i) transfer actuation forces onto the skin at various interface locations such that the skin profile deforms to its target shape, and ii) support the skin in resisting the flight loads. Actuators are selected based on the required stroke-force levels, available space and available input energy and it should be noted that this actuation selection is iterative with both the composite skin and compliant mechanism processes.

Figure 2 Geometry of the wingtip.

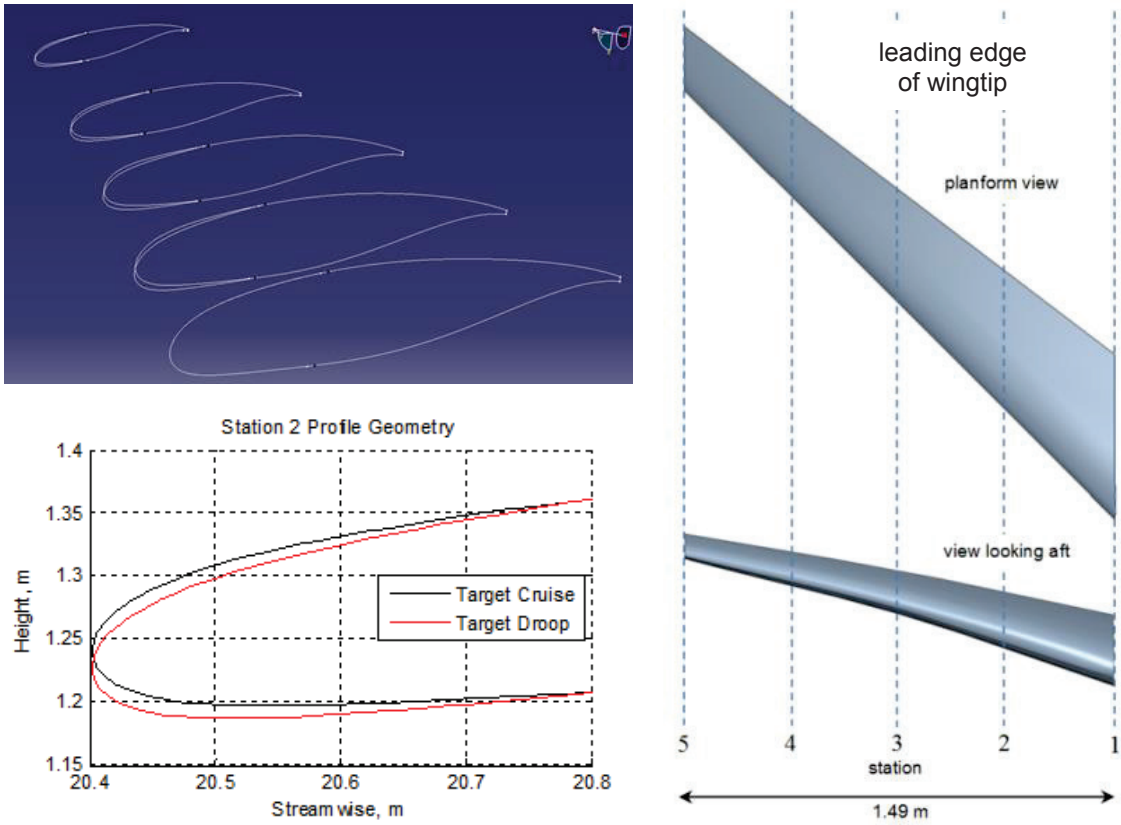

Figure 4 shows the components and the structural architecture of the droop-nose wingtip. Planar compliant mechanisms at two stations were chosen and a single ‘double L’ stringer was selected as the interface between the skin and the mechanisms due to the small droop target displacement (~ 2°). A planar form for the compliant mechanisms were selected for a number of reasons: i) manufacturing is relatively feasible through means such as laser, water-jet cutting or wire electrical discharge machining; ii) topology optimization can be performed in a 2D environment; and iii) material in

plate form tends to be more predictable in its behaviour as opposed to structures fabricated from additive manufacturing methods.

In terms of data flow, target shapes and aerodynamic load data (provided by Embraer) along with the skin material and plybook properties and actuator properties are used as input for the composite skin optimization process. The results of the skin optimization process are used as input for the compliant mechanism, wherein the design domain, interface connection points, and target displacements and the equivalent forces and stiffnesses at these interface points for the compliant mechanism are defined. Additional parameters such as the compliant mechanism material and thickness, actuator properties and boundary conditions, as specified by the user, are also input into the compliant mechanism design process. The results from both the skin optimization and topology optimization are post-processed for manufacturing, the parts manufactured and assembled.

Figure 3 Design chain of the DLR droop-nose morphing wingtip.

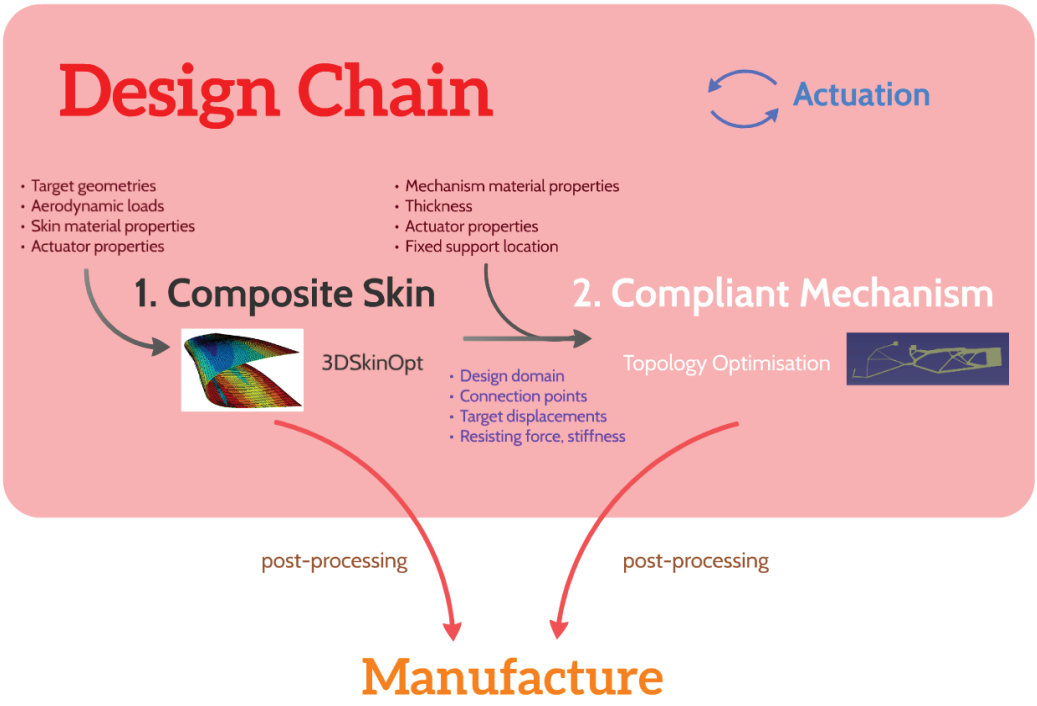

Skin Design

An optimization tool following that of Kintscher *et al*. (2011) was extended to a 3D environment and was used to design the skin. In this optimization tool, finite element models representing the wingtip in their different load configurations are solved and the results of these solutions are used as input for the optimization routine. This optimization tool is iterative and data flow is automated between the ANSYS finite element solver and the MATLAB-integrated Simplex algorithm

(Lagarias *et al*., 1998). This optimization tool provides the tailored thickness distribution (i.e. stacking sequence of plies), position of the stringer (i.e. the actuation load introduction point on the skin) and the force level required at this interface. The overall procedure of this skin optimization tool is described below, and all routines are performed in MATLAB with the exception of the ANSYS finite element solutions:

1. Wingtip section geometries, aerodynamic loads, optimization design variables and user defined variables (stringer height and foot length, material properties, plybook look-up table) are read
2. The finite element mesh is generated through a series of Cartesian coordinate parameterizations and interpolations and extrapolations
3. Aerodynamic loads and ply sequences are mapped onto the elements in the final mesh
4. All mesh, load, elemental ply stacking and design variable data is written and exported to ANSYS
5. Nonlinear finite element solutions generated in ANSYS for three load cases, taking into account the droop and stiffness function requirements:
    a. droop, no aerodynamic loads: the design variable actuator force is applied and aerodynamic loads are excluded
    b. droop, with droop aerodynamic loads: the resultant displacements from the previous solution at the skin-mechanism interface are applied and aerodynamic pressures in the droop configuration are also applied
    c. clean, with clean aerodynamic loads: the skin-mechanism interface location is fixed and aerodynamic pressures in the clean configuration are applied
6. Finite element analysis results from ANSYS are written and imported back into MATLAB
7. Design variables are updated
8. If convergence is attained, the process is terminated. Otherwise repeat Steps 1-7

For this NOVEMOR wingtip design, 20 optimization design variables (DVs) were used as shown in Figure 5. DVs 1-16 represent the skin thickness at 21 locations along the leading edge surface (a uniform thickness in the stringer foot region was maintained for manufacturing reasons); DVs 17-18 are the stringer position along the streamwise perimeter length at span stations 2 and 4; and DVs 19-20 are the force magnitudes (representing the force transferred from the actuator

through the compliant mechanism). The skin thickness is bilinearly interpolated between the 21 locations and spline interpolation and extrapolation is used to generate the stringer across the span length. The skin material used was prepreg-based GFRP Hexcel HexPly® 913.

Figure 4 Structural architecture of the DLR droop-nose wingtip (compliant mechanisms not shown).

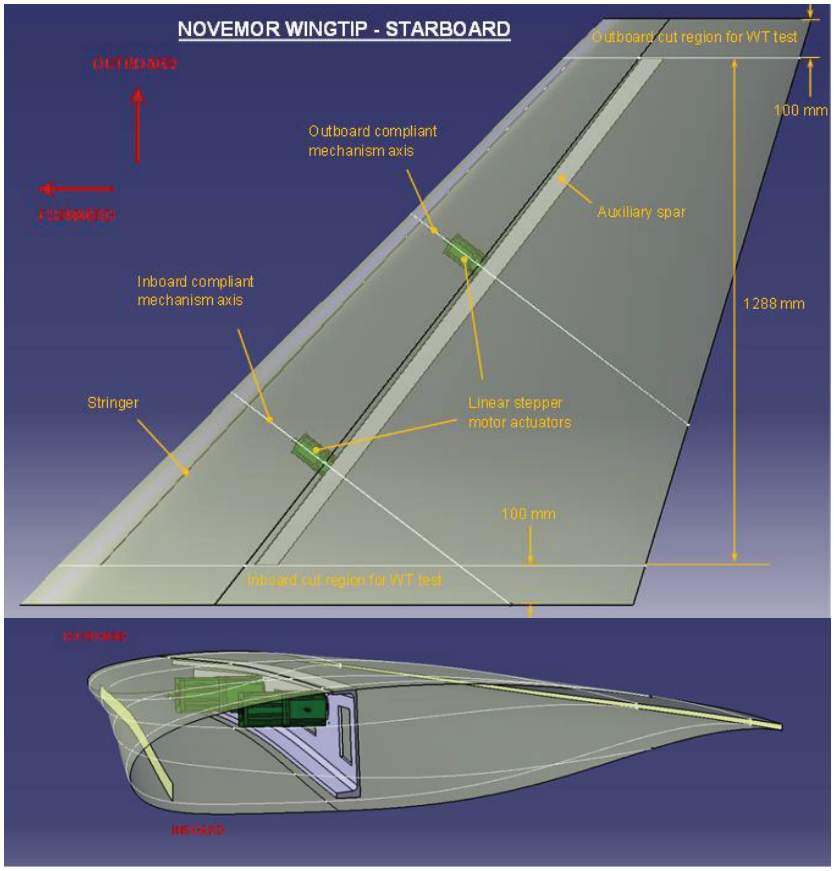

The objective function of the optimization was to minimize the sum of squared component position errors between the deformed P and target profile shapes $\tilde{P}$ (at N points along the station profile) at stations (index j) 2 to 5 for the droop case and stations 1 to 5 for the clean case as shown in Equation (1). The design variables were bounded from 1-4 mm for the skin thickness, 35-55 % of the station perimeter length for the stringer positions and 50-650 N for the actuation load.

The final thickness distribution is shown in Figure 6 and the profile displacements and objective function history are shown in Figure 7. It is clear that more material is distributed at the inboard and aft edges of the leading edge as was anticipated. Portions of the upper and lower surfaces of the skin at the tip feature low skin thickness (1 mm) with a larger thickness in the region between (i.e. the forward region) and this distribution could possibly be explained by the use of a uniform thickness in the stringer foot region. The objective function has smooth convergence over the course of the optimization process, and minimization of the shape error has been achieved for both droop and clean configurations. The maximum displacement error was approximately 5 mm in the clean configuration at station 1 as shown in Figure 7. This

maximum displacement error is relatively high and may be reduced by using higher bounds for skin thickness and actuator force. However, it is difficult to obtain actuators with higher force output that will also fit inside the tight space in the leading edge region. Thus this compromise was accepted and improvements could be made in accordance with actuator developments and further design iterations.

Figure 5 Design variables for the skin optimization process.

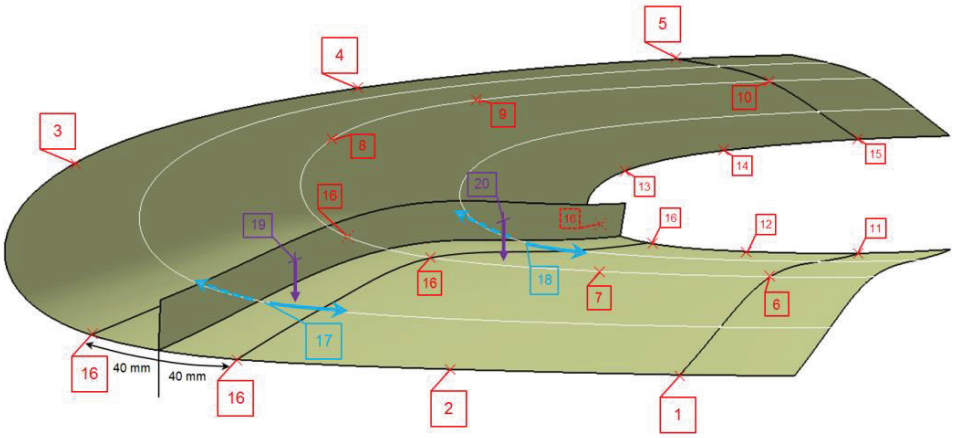

$$\min : \sum_{j=2}^{5}\sum_{i=1}^{N}\left(P_{droop_{i,j}} - \widetilde{P}_{droop_{i,j}}\right)^2 + \sum_{j=1}^{5}\sum_{i=1}^{N}\left(P_{clean_{i,j}} - \widetilde{P}_{clean_{i,j}}\right)^2 \quad (1)$$

Figure 6 Final skin thickness distribution of the DLR droop-nose wingtip (values in m).

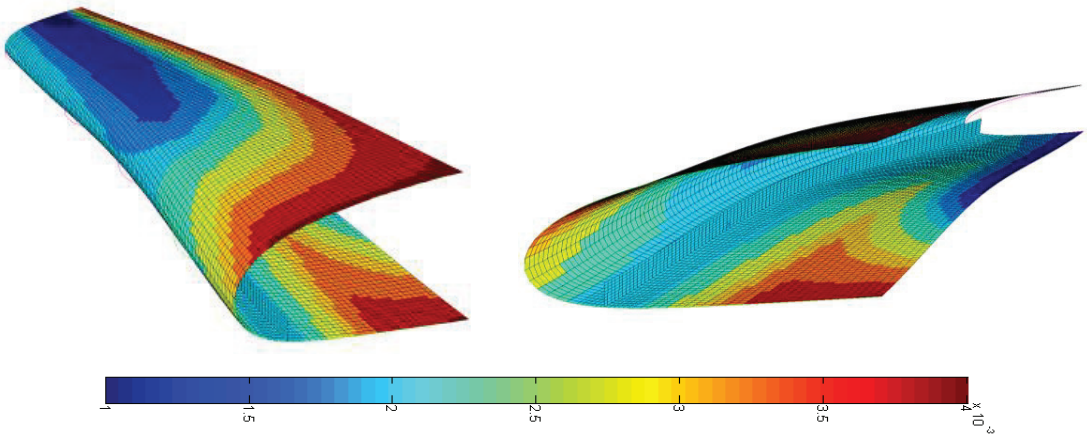

Skin Manufacture

The final skin design from the optimization was postprocessed where smooth contours of the thickness patches were generated using an ordered-edge detection method followed by a least squares 3D spline fit. The data was then exported

into a CAD program where the geometries of the 32 layers of the prepreg material were generated as shown in Figure 8. Due to the tight space inside the leading edge, manufacturing was performed in two halves (split at the stringer) as shown in Figure 9 and brought together using two curing stages. In this manner the layers in the stringer are integral and continuous with the layers going into the skin. The manufactured skin is shown in Figure 10 along with the aluminium 5083 auxiliary spar, milled from a single block of material.

Figure 7 Shape results: objective function and maximum displacement error histories; profile plots at stations 2-5.

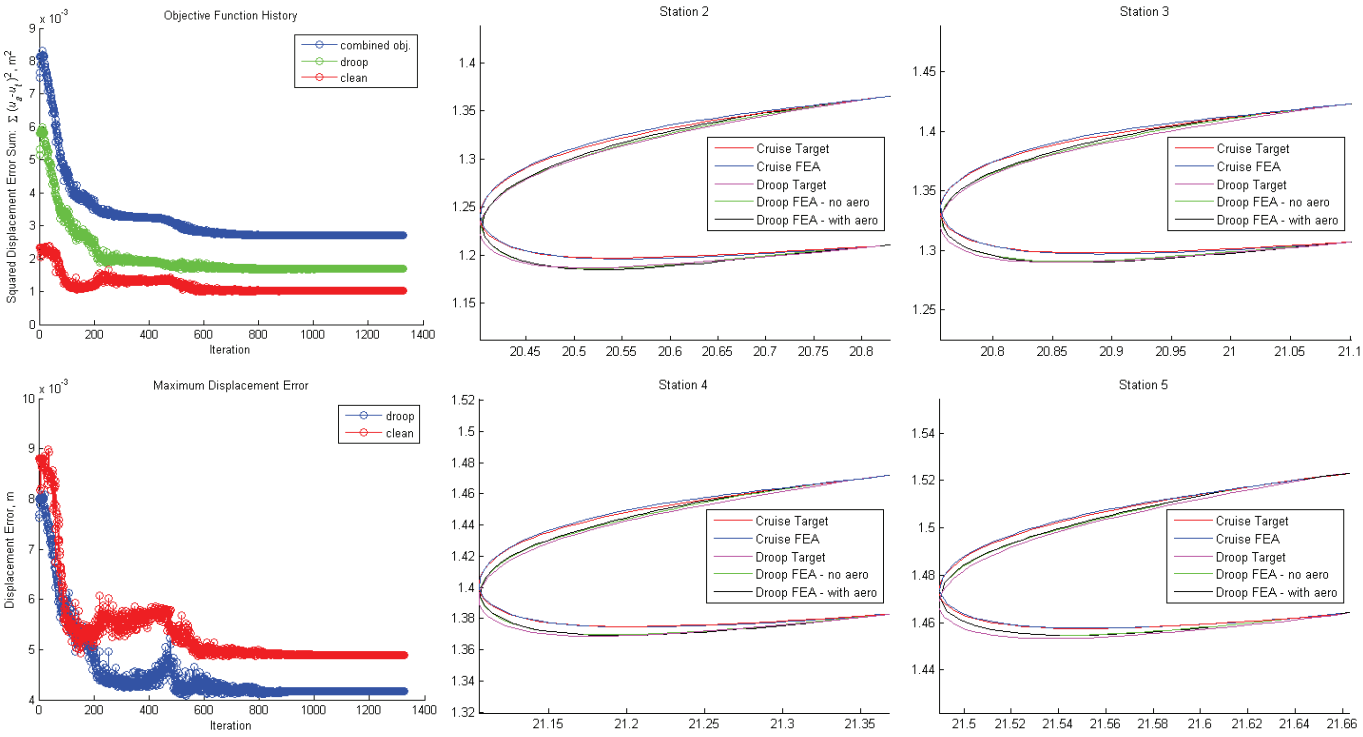

Figure 8 Ply geometry creation for skin manufacture.

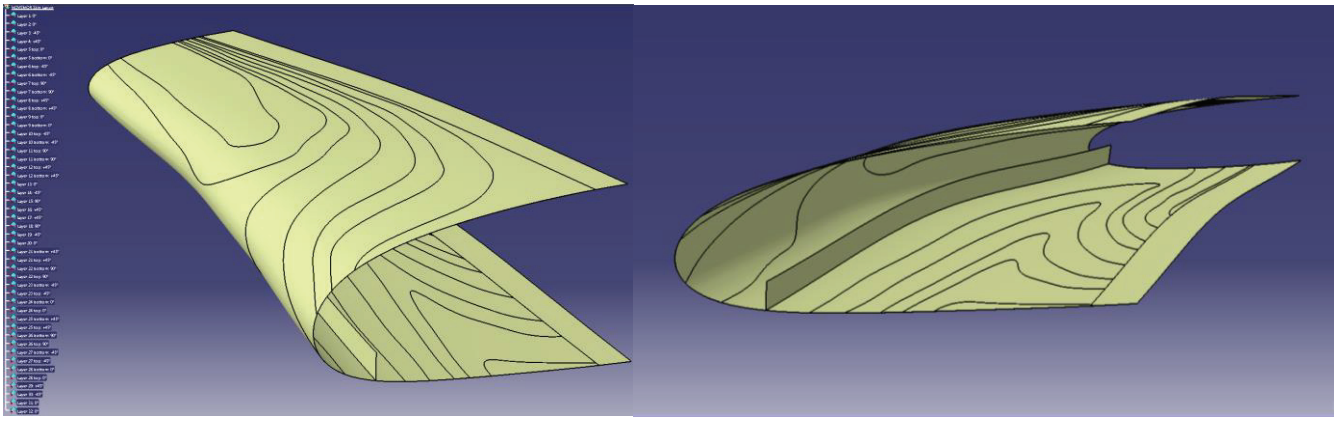

Figure 9 Composite skin manufacture method.

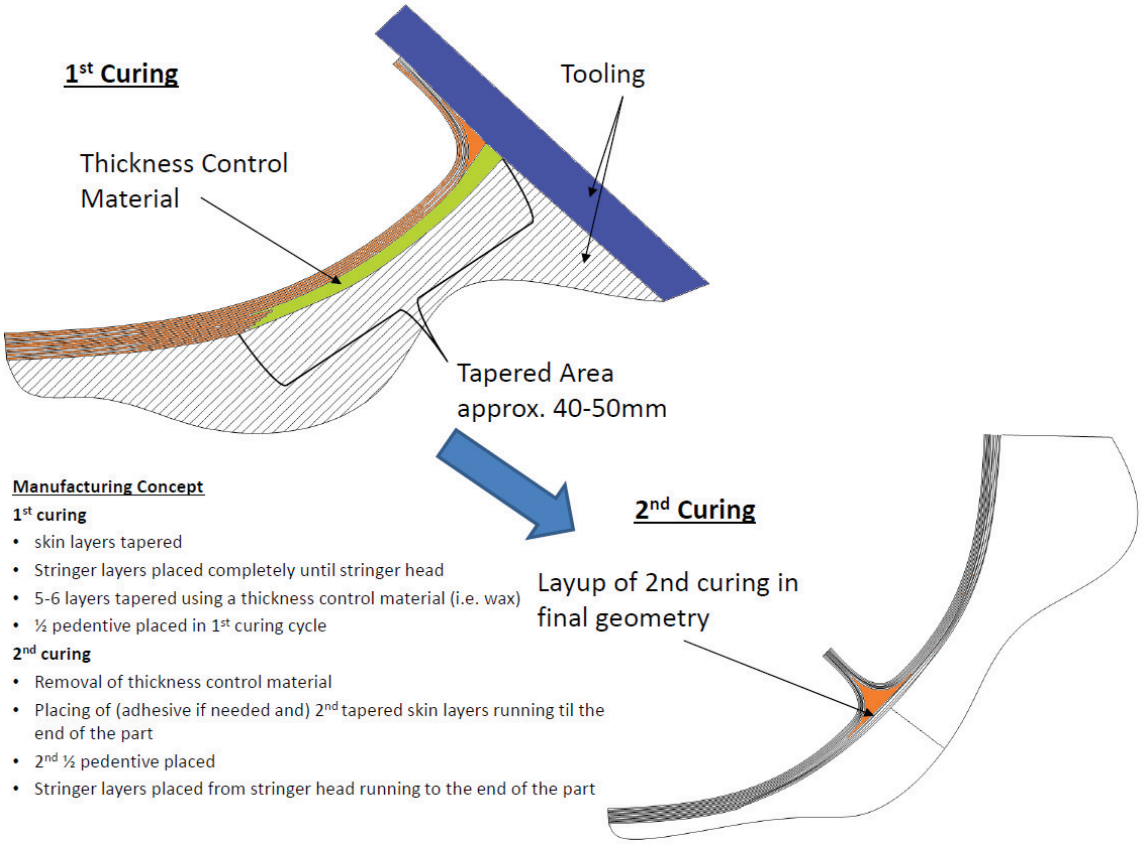

Figure 10 Manufactured composite skin placed on the manufactured aluminium auxiliary spar.

Compliant Mechanism Design via Topology Optimization

The purpose of the compliant mechanism is to transfer the force and displacement from the actuator onto the skin via the stringer in a precise manner when actuated thus drooping the skin, as well as to support the skin from adverse deformations due to external aerodynamic and inertial forces. The compliant mechanism works against the aerodynamic loads and the stiffness of the skin and these boundary conditions are obtained from the skin optimization results as per the design chain. The underlying rationale is that the skin will conform to its droop configuration if the mechanism displaces the skin (at the connection points) to their target positions, hence forming a precision-displacement shape control formulation for the mechanism optimization problem. Continuum gradient-based topology optimization with the solid isotropic material with penalization (SIMP) material model (Bendsøe, 1989; Zhou & Rozvany, 1991; Mlejnek, 1992) was used in this shape-control formulation to design the internal compliant mechanism. Different topology optimization methods have been previously used to design such compliant mechanisms and the usage can be loosely classed in three categories: i) use of the discrete load path representation and optimization update schemes such as genetic algorithms (Lu & Kota, 2005; De Gaspari & Ricci, 2011; Santer & Pellegrino, 2009); ii) the use of continuum gradient-based topology optimization methods for the bending shape control of plates (Kang & Tong, 2007; Luo *et al*., 2011); and iii) the use of continuum gradient-based topology optimization methods for the design of planar morphing structures (Santer & Pellegrino, 2009; Maute & Reich, 2006; Pedersen *et al*., 2001; Thuwis, 2012). This work can be classified in the last category and efforts have been made to develop an optimization routine capable of generating topologies which can be post-processed and manufactured, and in particular hinge-free, resulting in distributed compliance and improving the issues of stress concentrations and fatigue life. The design of the inboard compliant mechanism is described in this section and the material used was a superelastic nickel-titanium based alloy (effective elastic modulus of 70 GPa, Poisson's ratio of 0.3) due to its high strain capabilities. A linear finite element analysis routine was used in the topology optimization procedure along with the Method of Moving Asymptotes (MMA) (Svanberg, 1987) to update the design variables. A linear electrical stepper motor was placed horizontally with a maximum capable force of 1500 N.

The design domain and boundary conditions are shown in Figure 11 and the values of the parameters transferred from the skin optimization are shown in Table 1. The problem formulation as given in Equation 2 was to minimise the maximum elemental compliance in the set of compliances $\mathbf{C}$ in the clean configuration (denoted as subscript c), subject to constraints on the displacement errors between the deformed displacement u and the target displacements $\overline{u}$ constraints (i.e. the precision-control feature) in the droop configuration (denoted as subscript d) at the control degree of freedoms p. This setting of shape control precision as constraint functions instead of an explicit objective function follows the recommendation of Svanberg (2004). There is an additional material limit constraint where w is a prescribed fraction of

the design domain space. The design variables were the topological densities x and the actuator force magnitude normalised factor α. It should also be noted that the maximum actuator force was 1500 N, A is the element area, i denotes the current element and N is the total number of elements. In this manner, droop displacements and stiffness to external loads are considered, thereby forming a multifunctional compliant mechanism. It was also found for this case that this formulation led to a hinge-free solution

Figure 11 Topology optimization design domain and boundary conditions for the a) droop and b) clean configurations.

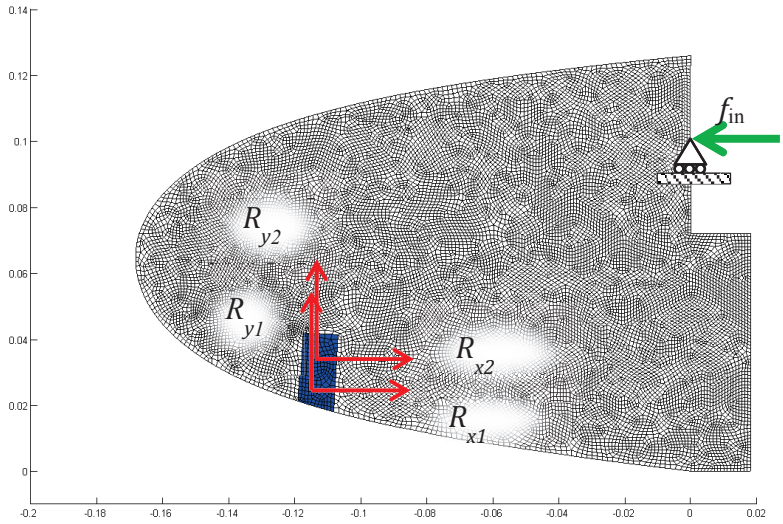

a)

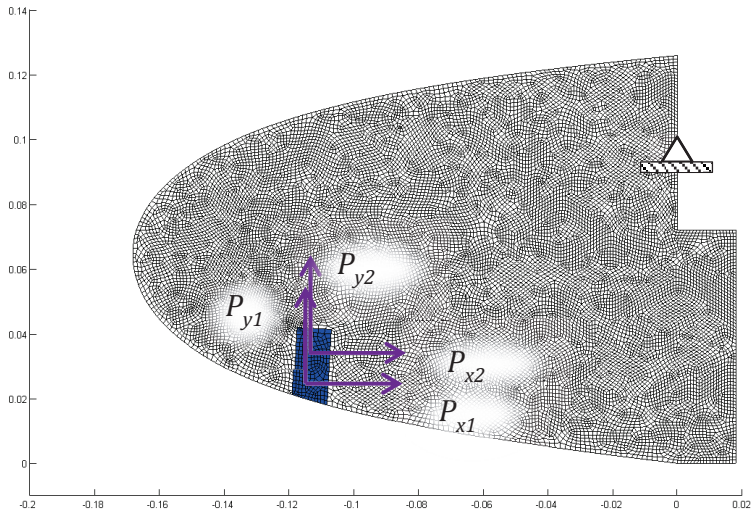

b)

.

$$
\begin{aligned}
&\min_{\mathbf{x},\alpha}: \max \mathbf{C}_c(\mathbf{x}) \\
&\text{Subject to:} \\
&u_{p_d}(\mathbf{x},\alpha) - \overline{u}_{p_d} \le 0 \\
&-\{u_{p_d}(\mathbf{x},\alpha) - \overline{u}_{p_d}\} \le 0 \\
&\frac{\sum_{i=1}^{N} x_i A_i}{w \sum_{i=1}^{N} A_i} - 1 \le 0 \\
&0 \le x_i \le 1 \\
&0 \le \alpha_{\min} \le \alpha \le 1
\end{aligned}
\tag{2}
$$

$\mathbf{C}_c$ is a matrix of the elemental compliances over the number of elements N and the number of clean load cases M:

$$
\mathbf{C}_c = \begin{bmatrix} c_{11} & \cdots & c_{1M} \\ \vdots & \ddots & \vdots \\ c_{N1} & \cdots & c_{NM} \end{bmatrix} \tag{3a}
$$

and

$$
c_{ij} = \mathbf{u}_{i_{j_c}}{}^{T} \mathbf{k}_i \mathbf{u}_{i_{j_c}} \tag{3b}
$$

The soft form for the maximum is used to approximate $\max \mathbf{C}_c$as shown in Equation 4 in order to convert the problem into a continuous differential one. The parameter β was gradually increased as per the continuation method from 1 to 5000 in 12 steps.

$$
\max \mathbf{C}_c \approx \mathbf{C}^* = \frac{1}{\beta} \log\left(\frac{\sum_j^M \sum_i^N e^{\beta c_{ij}}}{MN} \right) \tag{4}
$$

Table 1 Values of parameters in the topology optimization routine.

Parameter	Value
f_{in}	1500 N (max)
$\overline{u}_{1_d}$	-1.054 mm
$\overline{u}_{2_d}$	-11.47 mm
$\overline{u}_{3_d}$	-0.88 mm
$\overline{u}_{4_d}$	-11.45 mm
R_{x1}	190 N
R_{y1}	390 N
R_{x2}	190 N
R_{y2}	390 N
P_{x1}	231 N
P_{y1}	-200 N
P_{x2}	231 N
P_{y2}	-200 N

Figures 12 a and b show the resultant topology in the clean and droop configurations respectively and the topology features beam-like members of varying lengths and thicknesses. The absence of artificial hinges results in a more distributed compliance as shown in Figures 12 c and d resulting in lower stress concentrations. The absence of hinges also enables a much easier postprocessing phase as the topology boundary is more clearly defined and the mechanism performance is not highly sensitive to small topology variations at a local region, as associated with hinged compliant mechanisms. The displaced topologies show very close matching to the target points for the droop case, and almost zero displacement to the external forces for the clean case, indicating that the stiffness and flexibility functions have been achieved. The objective function history plots in Figure 13 show minimization of the compliance, the sum implicitly in Figure 13b and the maximum explicitly in Figure 13c, and shape control error over the optimization iterations in Figure 13a with a final displacement error in the order of 1 mm^2. The input actuator displacement is approximately 8 mm and the input force was 1500 N as shown in Figure 14.

Figure 12 Topology optimization results: topologies and displacements in the a) clean and b) droop configurations. Compliances in the c) clean and d) droop configurations.

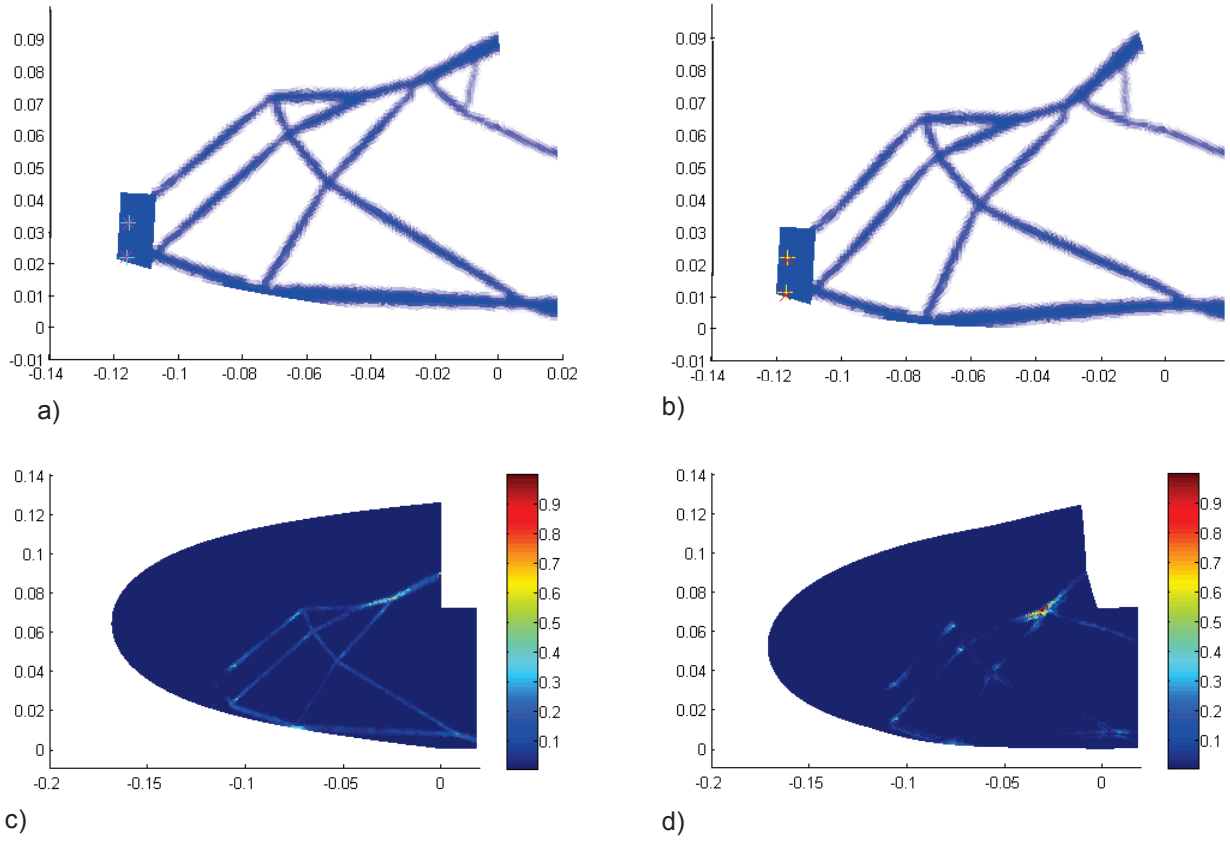

Figure 13 Topology optimization objective function results. a) shape control objective; b) implicit compliance sum objective; and c) explicit maximum compliance objective.

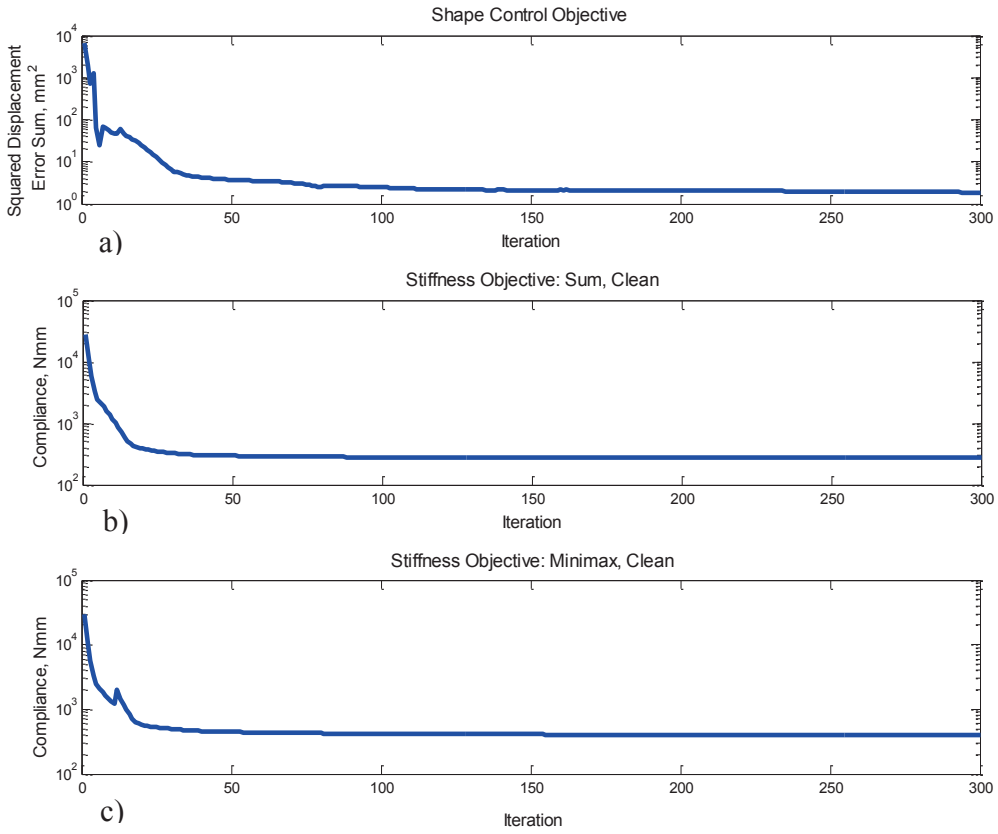

Figure 14 a) Input displacement and b) force histories in the topology optimization process.

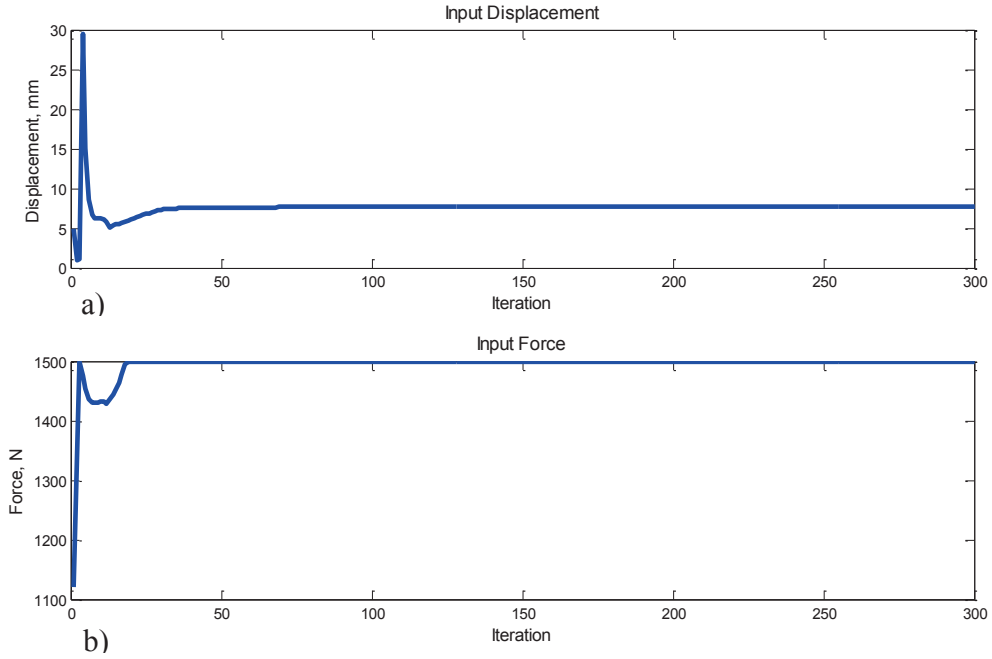

Compliant Mechanism Manufacture

The compliant mechanism was manufactured from superelastic nickel-titanium alloy in 5 mm thick plate form using wire electrical discharge machining. The photo of the manufactured mechanism is shown in Figure 15a and Figure 15b shows the mechanism attached to the actuator before assembly into the leading edge skin and spar.

Figure 15 a) Manufactured compliant mechanism and b) attachment to actuator and assembly support jig.

a)

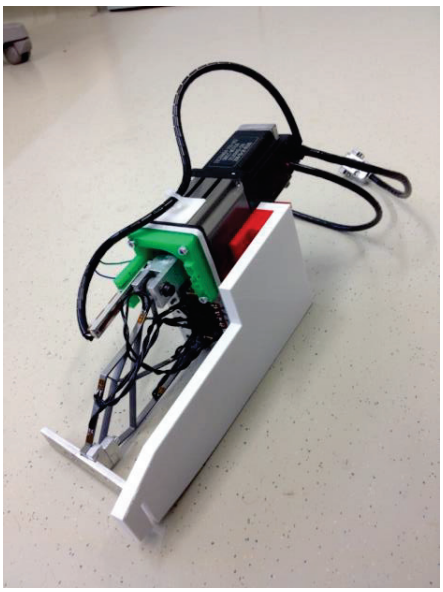

b)

Wind Tunnel Testing

As mentioned, the manufacture of the droop-nose wingtip was undertaken for wind tunnel testing at the University of Bristol low speed subsonic facility. The wingbox and trailing edge of the wingtip was manufactured by the University of Bristol and assembled with the morphing leading edge. Figure 16 shows the assembled wingtip mounted in the wind tunnel ready for testing. The testing scheme is currently underway and as such the testing results will be disseminated in the future and only the testing aims and instrumentation are provided here.

Figure 16 NOVEMOR droop-nose morphing wingtip mounted in the wind tunnel.

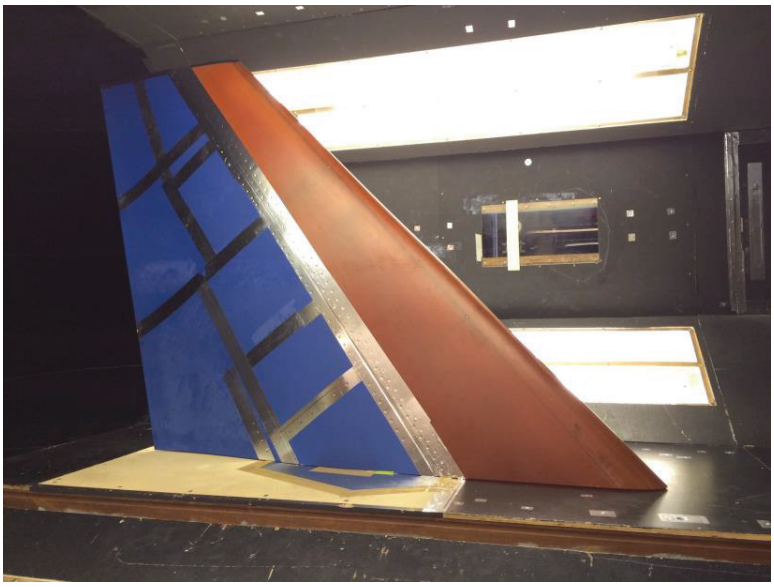

The wind tunnel test section is 2.1 by 1.5 m and a maximum flow velocity of 55 m/s. The test matrix involves running three different droop settings (0%, 50% and 100% droop) at speeds from 25 to 55 m/s at 5 m/s increments and angles of attack from -10° to +10° at 2.5° increments. It should be emphasised that the testing was not conducted with the aim of quantifying lift/drag benefits, but to subject the morphing structure to aerodynamic loads and assess the structural performance. The instrumentation used in the testing includes: a) strain gauges placed on the skin and mechanisms all in quarter-bridge configurations (6 on the skin, 6 on the inboard mechanism and 2 on the outboard mechanism); b) 61 pressure tappings at one section along the span (39 on the leading edge, 22 on the wingbox/trailing edge structure); c) external displacement sensors measuring the actuator stroke (one per actuator); d) wind tunnel load cell balance providing force moment information; e) 2 internal cameras providing video information. Measurement of the droop surface shape was not possible inside the tunnel and was performed outside in separate ground tests. Specifically, the aims of the wind tunnel test are as follows:

- assess the feasibility of the DLR morphing droop-nose under aerodynamic loads
- measure the strain levels in the skin and compliant mechanism
- validate the skin optimization and topology optimization design methodology
- measure the pressure distribution along one station for comparison with CFD simulations for the purpose of validating the analysis and providing loads back to structural FEA simulations to assess the displacement, strain and stiffness behaviour of the morphing structure when extrapolated to loads at higher flow speeds.

POLIMI Morphing Leading and Trailing Edge Devices

Compliant mechanisms for leading and trailing edge were obtained using two main tools dedicated to the morphing aircraft design, named PHORMA and SPHERA. The general approach is based on a geometry parameterization, based on CST method (Kulfan, 2008), coupled to a two levels optimization procedure (De Gaspari, 2010; De Gaspari & Ricci, 2011). In the first level the best deformed airfoil shape is determined as the most efficient aerodynamic shape which at the same time limit the requested energy to deform the airfoil skin. In the second optimization level the best internal structural configuration is obtained using a topology optimization tool based on genetic algorithms that synthesizes a compliant structure able to adapt itself for matching the optimal shape coming out from the first level. While SPHERA (Synthesis of comPliant mecHanisms for EngineeRing Applications) is a general tool for the synthesis of compliant mechanisms, with specific features dedicated to the design of morphing wing, all the parametric capabilities, able to handle the models, are inherited from PHORMA (Parametrical sHapes for aerOdinamic and stRuctural Modelling of Aircrafts) that represents an integrated multiphysics environment, based on the CST parameterization. Once aeronautical 3D geometry is identified and corresponding parameterized shapes are available, different models can be linked to a common geometry representation. The framework includes features for the generation of CAD, CFD, FEM and load paths models and contains techniques for the coupling between the different models. The parametric shapes can be combined and directly used to produce corresponding mesh, to perform structural and fluid analyses and to provide a fast interface to commercial softwares. The most important parts have been implemented as objects and classes interacting each other by means of the Object—Oriented Programming (OOP). The OOP concept allows an independent development of each component and an easy interface with any other application which can take advantage of its capabilities.

One of the main classes in the framework is the OOP—based PFEM class which incorporates an in—house FEM code able to handle different types of elements and incorporate different solvers. As well as SPHERA is an object that inherits the PFEM properties to solve structural problem corresponding to the Load Paths representation, PHORMA is an object based on different sub—classes which interacts with PFEM methods to generate 3D aeronautical FEM models. PFEM incorporates modal, buckling, linear and non—linear static analyses, allows to use different types of elements and provides several methods containing standard tools for the management of a FEM model. In addition to the basic BAR element and to some iso—parametric element, such as Q4 bilinear quadrilateral element, the code includes Finite Volume Beam element (Ghiringhelli *et al.*, 2000). The Finite Volume C0 Beam is a particular type of non—linear beam, usually adopted as deformable connection component in the multibody applications.

PHORMA is coupled with the PFEM to produce different parts of aircraft structures, such as wingbox, skin, ribs and stringers components. At the same time it is also coupled with SPHERA to add morphing devices in terms of 3D FEM

models of compliant mechanisms. Different classes can be used as pre-processing and post-processing during the design of compliant mechanisms. All these interactions can be used to compute aerodynamic loads or to generate complete 3D FEM models with embedded compliant mechanisms devices, as shown in Figure 17. The aerodynamic loads can be applied to the load path models during the synthesis of compliant mechanisms or directly to the final 3D FEM models. In the first case, the aerodynamic loads can be directly computed on the 2D airfoil corresponding to the compliant mechanism or extracted from 3D analysis results.

Aerodynamic loads acting around a single wing section are computed by a specific code embedded into the CST tool able to automatically produce a 2D structured mesh around the airfoils and to perform Navier-Stokes computations. The automatic generation of the structured mesh around the parameterized airfoil shape is based on a script for Ansys ICEMCFD. It is represented by a Tcl/Tk shell with an extended library consisting of ICEMCFD commands, while CFD computations are performed by means of EDGE code. Once the CFD analyses have been performed, the CST tool is able to extract the results in term of Cp distribution and to spread them along the airfoil shape used to produce the compliant mechanism models. While the optimal morphing mechanisms is computed at first on the 2D airfoil, then extended to the full wing, it is important that the aerodynamic loads considered during the 2D optimization are representative of the 3D wing. For this reason the aerodynamic loads can be also directly extracted from 3D CFD computations. Once the 3D model is obtained in a parametrical way, unstructured surface meshes can be generated completely without user intervention. Geometric refinement criteria produce a finer mesh in regions of strong curvature, such as morphing leading edge region. Unstructured or hybrid volume meshes can be generated from the surface mesh and used to perform Euler or Navier—Stokes computations. Afterwards PHORMA is able to extrapolate the aerodynamic results, around one or more sections arbitrarily positioned and oriented, and to match them to corresponding CST parameterized shapes. The post-processing class includes an interpolation technique able to match 3D data results with the sections parametrically identified. Once the aerodynamic results are computed, a fluid—structure interaction (FSI) method, based on the Radial Basis Function (RBF), is available in the procedure to transfer these loads from the aerodynamic mesh to the structural grid points placed on the wing skin.

The parametric framework, briefly described in this section, can be coupled to dedicated shape optimization procedure for the definition of the optimal morphing shapes and then to SPHERA for the synthesis of compliant mechanisms.

Figure 17 FEM mesh generation of a compliant wing and CFD loads transferring.

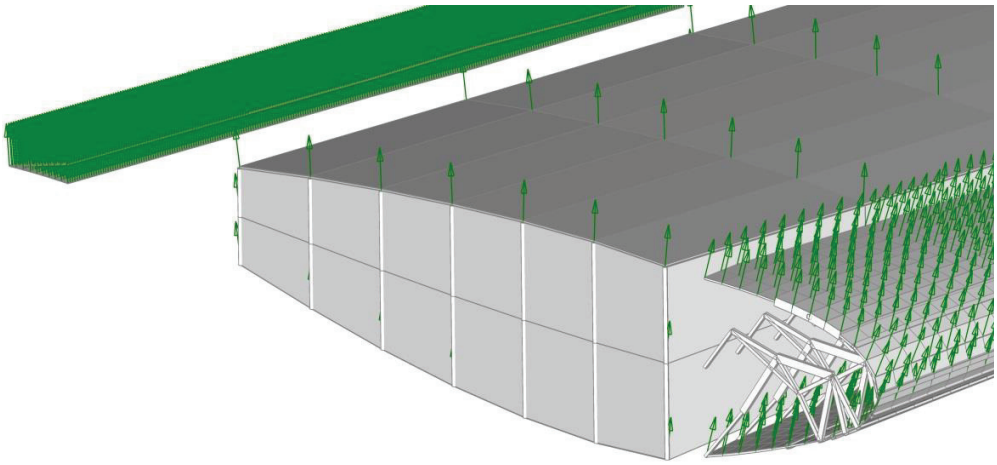

Aero—structural Shape Optimization

The shape optimization aiming at the definition of the optimal morphing shape is coupled with PHORMA both to compute the structural stresses along the skins and to generate the CFD models for the aerodynamic performances evaluation during the process. After the parametric model is generated, it results analytically defined and its shape can be easily controlled. In general, the shape optimization is used to guarantee that the morphing aircraft has optimal aerodynamic characteristics over one or more flight conditions, under structural skin constraints based on the geometrical quantities previously defined.

In this work the approach has been applied to one of the wing sections of the NOVEMOR Reference Aircraft which has been used to produce a scaled untapered morphing wing, tested in the wind tunnel of PoliMi. The shape optimization used to introduce morphing shape changes into the reference model can be performed by a 2D structural shape optimization, where only structural constraints are satisfied along the skin, that can be coupled with an aerodynamic shape optimization able to evaluate the performances in 2D. Two nested optimization loops are used so that the aerodynamic performances are evaluated only on the physically acceptable shapes. The 2D shape optimization is represented in Figure 18.

Figure 18 Scheme of the aero—structural optimization based on the 2D parametric structured mesh interface

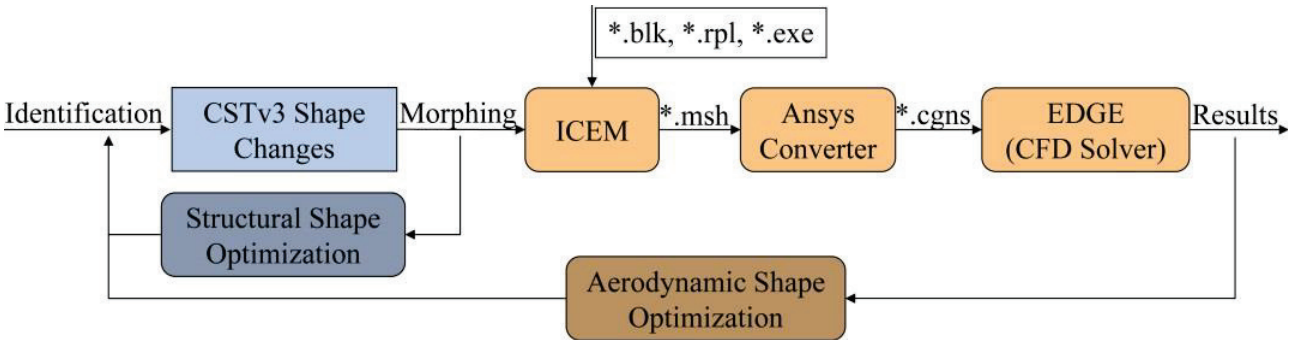

The objective function consists of minimizing some aerodynamic performance index, like the aerodynamic efficiency *L/D*, under different kind of constraints. Looking at a single wind tunnel test speed equal to 40 m/s, this procedure has been applied to obtain the optimal aerodynamic shape which are shown in Figure 19, together with the aerodynamic pressure distribution along the airfoil chord. In particular, in the case of the leading edge, the 2D aerodynamic optimization aims at the maximum efficiency while, as structural constraint on the skin, a null length variation so to minimize the axial stresses is used. In the case of the trailing edge, the 2D aerodynamic optimization aims at the maximization of the CL with a limitation on the maximum skin deformation.

Figure 19 Optimal morphing shapes (right) and corresponding aerodynamic C_p distributions (left) coming from the described shape optimization procedure based on RANS computations.

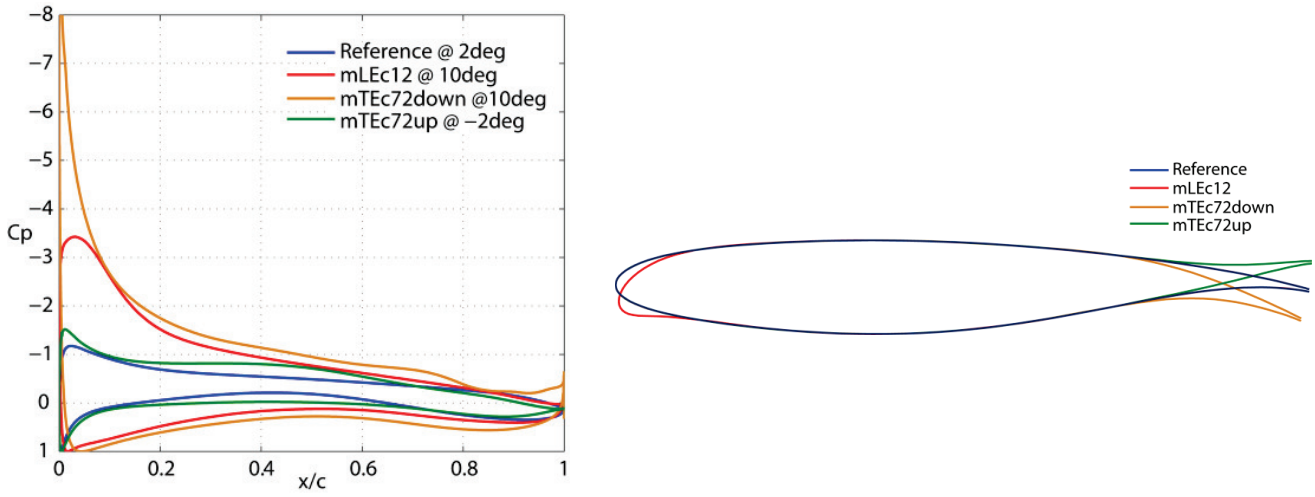

The Synthesis of Compliant Mechanisms for the Design of the Morphing Wind Tunnel Model

Morphing wings include the skin, a structure and a mechanism. Any process to design a morphing airfoil must simultaneously include these elements. SPHERA allows to conciliate the conflicting requirements of deformability, load–carrying capability and low weight design systems by means of the synthesis of compliant mechanisms based on the distributed compliance concept. It is based on the load path representation which is a structural parameterization technique that allows to unify structural topologies, cross–sectional sizes and shape problem (Lu & Kota, 2005; De Gaspari, 2010). This approach is valid for the synthesis of generic compliant mechanisms and it can be successfully applied to the design of adaptive structures for the shape control.

The code has been applied to the optimization of compliant structures adopted to equip the NOVEMOR wind tunnel model. Figure 20 shows characteristic points and target curves of the considered NOVEMOR airfoil: the chord extension of morphing devices is equal to 12% for the compliant leading edge and 72% for the compliant trailing edge. The design started with sensitivity studies on the position of the input actuator and the set of the active output points placed along the skin.

Figure 20 Load path representation (SIMO) of the NOVEMOR compliant leading and trailing edge and corresponding four types of characteristic points: active output points (cyan), deactivated output points (black) for the external load application, internal structure points (red), input actuation point (yellow), and constraint points (blue).

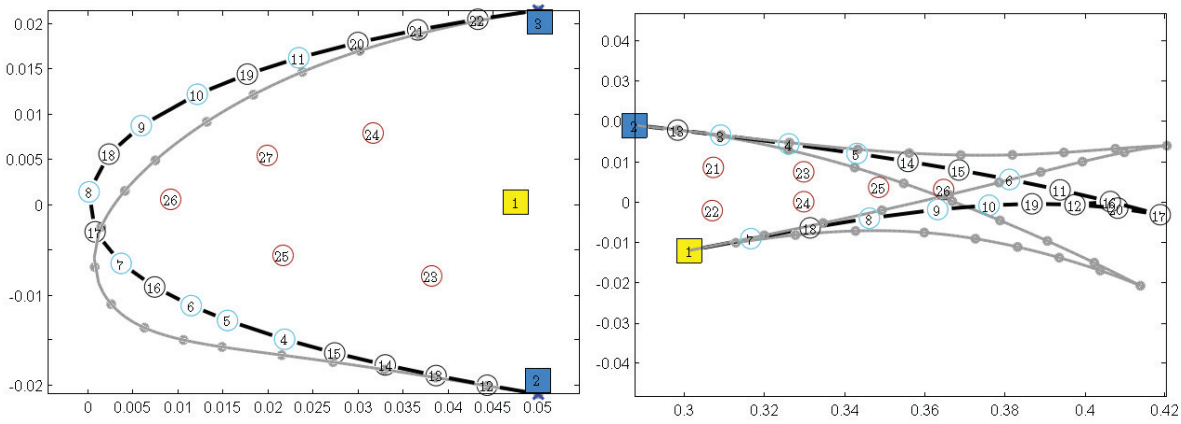

The design variables include user—defined path sequence, corresponding binary path existence variable, a total of 5 pairs of internal point coordinates for the leading edge and 6 for the trailing edge, the cross sectional load path sizes, a total of 8 load path output destinations and the structure boundary sizes. A number of points placed along the skin contour, equal to 19 for the leading edge and 18 for the trailing edge, is used to minimize the Least Square Error (LSE) between the deformation and the target curve which comes out from the shape optimization described in the previous section. The optimization problem tries to minimize the least square error under size constraints for the load path beam

elements and the structure boundary elements compatible with the manufacturing technology that will be adopted to produce the wind tunnel model. Since 3D printing technologies have been used for producing the leading and trailing edges, a close relationship with the company involved in the production of the morphing parts led to choose a minimum design thickness equal to 0.5mm.

Once the CST model of the target shape is available, it allows to identify the optimal position of the active output points and helps to compute the external aerodynamic load. Morphing airfoil meets the load–carrying requirement if they are able to adapt their shape and to maintain it under the external aerodynamic load corresponding to the same flight conditions. SPHERA inherits the interaction between the mechanism/structure and the fluid by means of the technique described in the previous sections, in order to build a coupling between structural and aerodynamic models.

Genetic Algorithms Based on Multi-Objective Optimization Problems

Because the deformation of the wing skin is influenced by both the topology and the dimensions of the compliant mechanism, it is important to unify and simultaneously address the topology and size design of the airfoil structure. For this purpose, SPHERA incorporates a customized Genetic Optimizer where the individuals making up the population, are composed by mixed–type design variables and the generation of each new population is produced by selection, crossover and mutation dedicated strategies which represent the kernel of the whole design tool. Writing dedicated selection, crossover and mutation subroutines allows to combine the topology synthesis, the size and shape optimization into the same process, by imposing connectivity, stress and buckling constraints simultaneously.

Moreover, in order to design a compliant mechanism able to meet both kinematic (motion) and structural (load–carrying) requirements, the design must be decomposed into several parts considering the mechanism design and the structure design, respectively, for a number of flight conditions corresponding to the design conditions. This is a typical multi—objective design problem that can be efficiently incorporated into the genetic algorithm (De Gaspari & Ricci, 2014).

Most real world optimization problems usually involve multiple objectives, where different solutions may produce trade—offs among them. A solution that is optimal with respect to one objective requires a compromise in other objectives. On the other hand, Genetic Algorithms can find multiple optimal solutions in one single simulation run due to their population-approach. Thus, they are ideal candidates for solving this multi—objective optimization problems. The approach hereafter used for solving this kind of problems applied to our purposes is the so called Elitist Non-Dominated Sorting Genetic Algorithm (NSGA-II) (Deb *et al.*, 2002).

The synthesis of morphing airfoil is defined as the design of a structure able to convert a displacement or a force in order to efficiently transfer the deformation work from an input point (actuator) to the output points placed along the skins.

This requirement is only kinematic, and additional structural requirements are necessary in order to maintain the undeformed or deformed shape under external loads. In general, more than one load conditions corresponding to the undeformed shape and more than one target shapes corresponding to different flight conditions can be considered. On the one hand, the morphing airfoil internal configuration which minimize the LSE (Least Square Error) is one that maximize the virtual work required because the displacements of the output points allow to match the desired airfoil shape change, under the input actuation load and the external aerodynamic loads corresponding to a given flight condition. On the other hand, the structural requirement can be met by solving a system where the input point is fixed and the external aerodynamic loads are applied along the airfoil skins. Minimizing the LSE between the deformed curve and the undeformed airfoil allows to account for the resistance of the workpiece.

When SPHERA tool is applied to the morphing leading or trailing edge of the wind tunnel model, multiple objectives have been considered. The minimization of the SE (Strain Energy), solving a system where the input point is fixed and the external aerodynamic loads correspond to the undeformed shape placed at 2° of angle of attack (structural requirement); the minimization of the LSE because the displacements of the output points allow to match the target shape changes defined by PHORMA, under the input actuation load and the external aerodynamic loads corresponding to the same target shape and to the considered test condition with 10° of angle of attack (kinematic requirement). Once obtained the optimal shapes from the shape optimization, the framework SPHERA has been adopted to define the optimal internal compliant structure able to produce, once actuated, the desired external shape.

In the case of leading edge, a standard multi—objective problem has been setup, combining one kinematic and one structural requirements. Figure 21 shows Pareto Front solutions obtained for the previously introduced leading edge and the selected design point. In particular the point highlighted with red color represents the best compromise between the two objectives and shows a LSE value of 3.9e-4 m with respect to the red target shape of Figure 19.

In the case of trailing egde optimization, due to the double kinematic requirement of moving the surface up and down (yellow and green curves in Figure 19), the multi—objective function has been selected by combining the kinematic constraints (LSE error between the actual and the target shapes), in both up and down configurations, with the structural requirement. For this reason the Pareto Front represents a three—dimensional surface shown in Figure 22 where the trailing edge design points is also reported. The compliant trailing edge guarantees a LSE values of 6.e-4 m for the downward deflection and 5.e-3 m for the upward deflection. These values are justified because the downward deflection and the structural requirements have greater priority than the upward deflection during the wind tunnel tests.

Figure 21 Pareto Front and design point for the leading edge device.

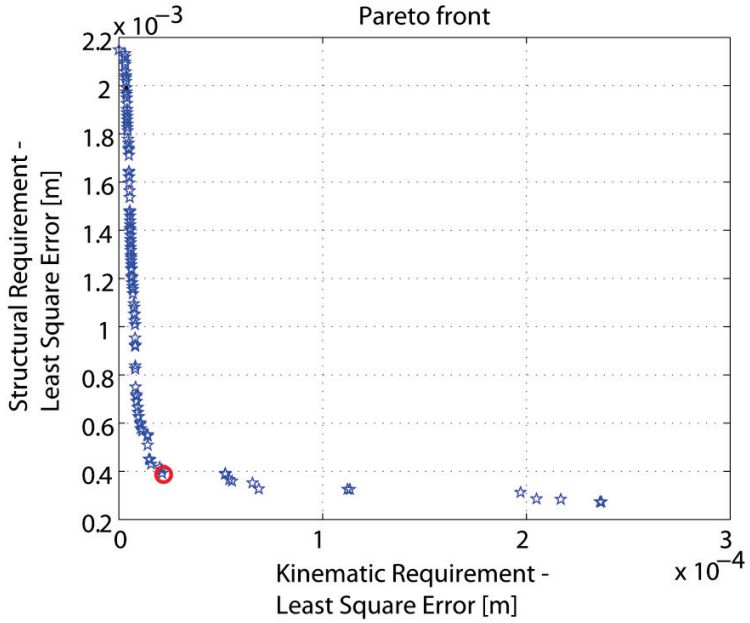

Figure 22 Pareto Fronts and design point for trailing edge device.

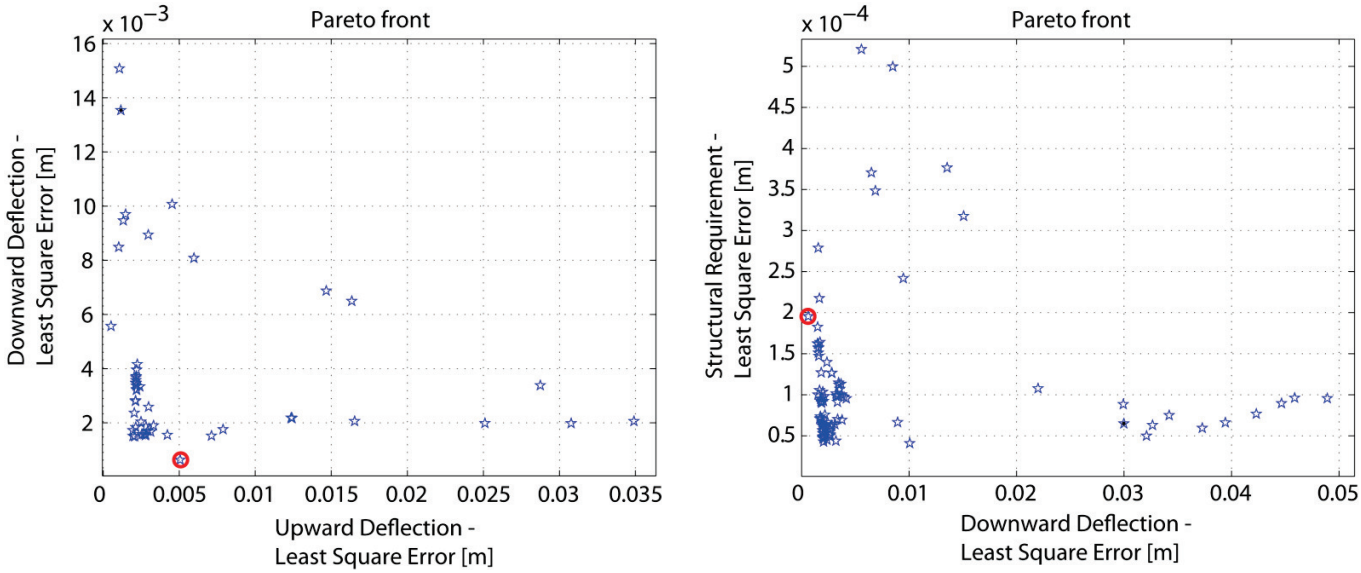

The optimal design of the compliant leading edge, together with the comparison between its deformation and the target shape, and the corresponding aerodynamic field computed for target shape in the wind tunnel condition are shown in Figure 23. Low—fidelity and high—fidelity 3D FEM models have been generated in order to validate the 2D solutions coming out from the Pareto Front. Figure 24 shows a 3D hybrid model where glued contacts have been used for the connection between the mesh of each adaptive rib, composed by tetrahedral elements, and the mesh of the skin, composed by plate elements. The Von Mises stress distribution into the rib showed an excellent correlation with the 2D Finite Volume Beams—based model. The structure is driven by a single rotor actuator that introduces the desired linear

displacement by means of a rod. Because the compliant leading edge matches the target shape a rotation of 10° is required.

Figure 23 The optimal compliant leading edge: aerodynamic loads corresponding to target shape (left) and compliant structure stress/deformation field (right) obtained on the 2D Finite Volume Beams model used by genetic algorithm.

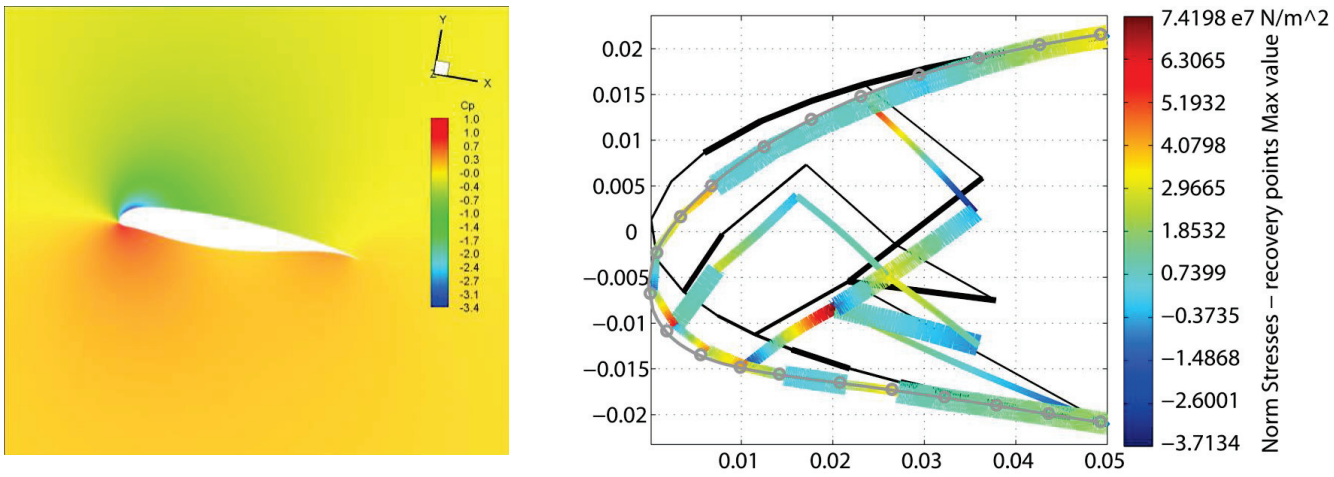

Figure 24 High—fidelity 3D FEM results of the morphing leading edge device.

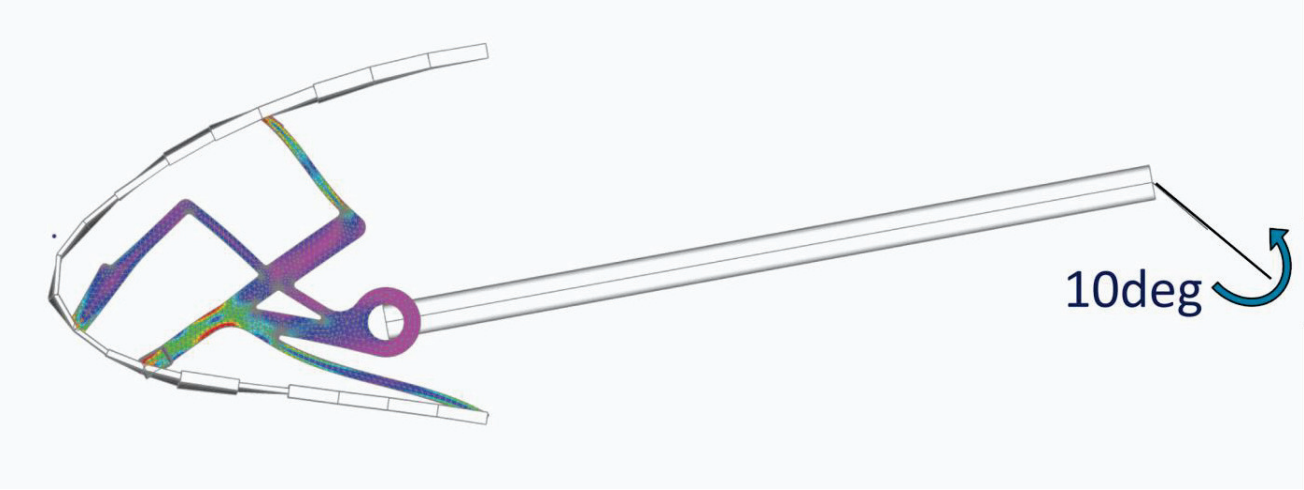

The optimal design of the compliant trailing edge in both maximum up and down configurations, together with the two corresponding load conditions computed for the target shapes in the wind tunnel conditions, are shown in Figure 25. Figure 26 shows a 3D hybrid model generated by PHORMA using beam elements for the rib models and plate elements for the skin model. The structure is driven by a single linear actuator applied to the lower skin able to slide along its parallel direction. Because the compliant trailing edge matches the target shape, linear displacements of 4 mm are required.

Figure 25 The optimal compliant trailing edge: aerodynamic loads corresponding to the two considered target shapes (left) and compliant structure stress/deformation field (right) obtained on the 2D Finite Volume Beams model used by genetic algorithm.

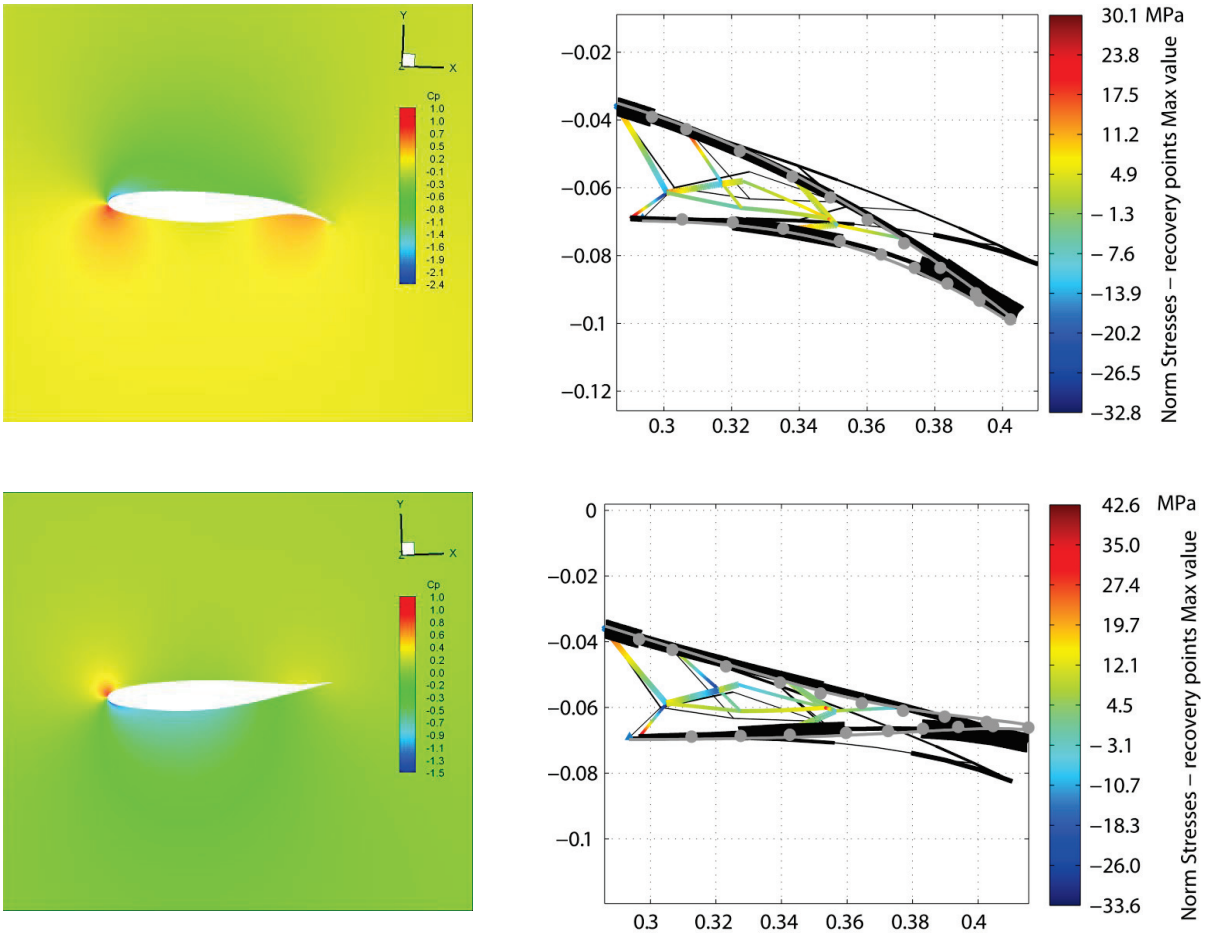

Figure 26 3D FEM results of the morphing trailing edge device.

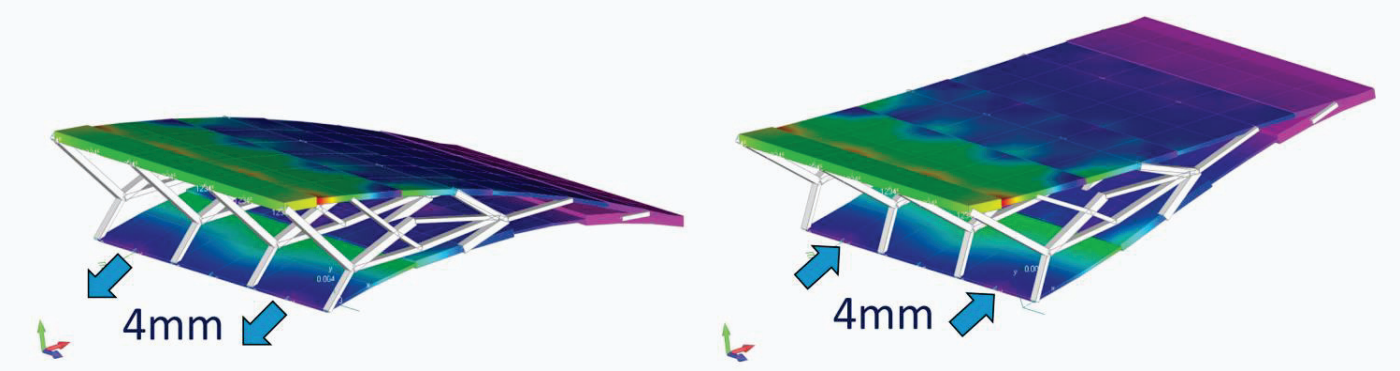

Once the 3D design of the compliant structures is completed, corresponding CAD models, shown in Figure 27, have been generated and directly provided to the company that is in charge of the morphing parts manufacture by means of 3D printing technology.

Figure 27 CAD models of compliant leading and trailing edge devices for the manufacture by 3D printing.

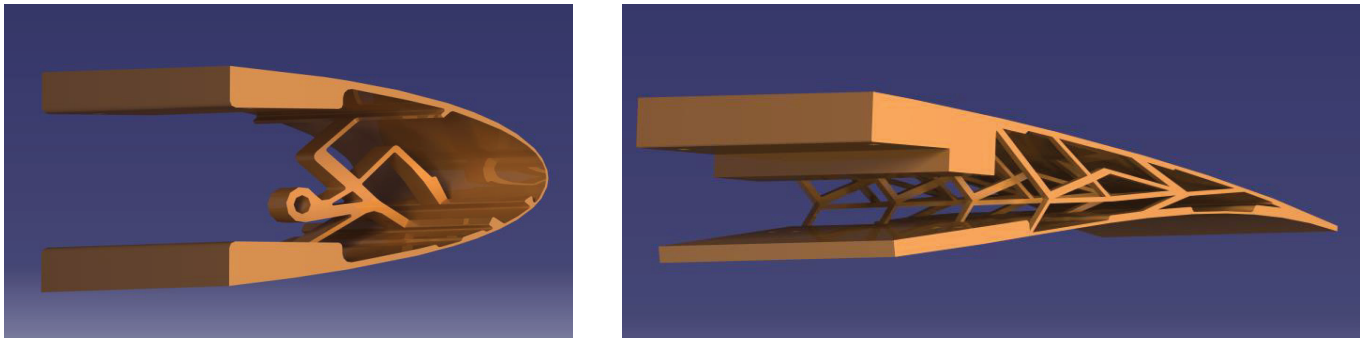

Wind Tunnel Testing

The experimental campaign aimed at the validation of the optimization procedure to design the compliant devices able to produce the optimal morphing shape. This campaign is under way and the first results about the quality of the morphing shapes reached during the wind tunnel tests performed at 40m/s, together with the models and methods adopted, are reported in the following.

It appears as clearly understandable that it is not possible to take the compliant structure designed for full aircraft and simply down scale it to the right size available in the wind tunnel. It is necessary to redesign completely the morphing structures working directly on the real size of the wind tunnel model. The wing model here considered has to be tested in the small scale wind tunnel available at PoliMi, equipped with a testing chamber of 1x1.5x3 m for a maximum speed of 55 m/s. It is shown in Figure 28 together with the morphing wing model. The wing model has a span of 1m and a chord of 0.417m. As already mentioned, in order to reduce the complexity of the experiment, the wing is untapered.

Figure 28 The wind tunnel used for morphing devices validation at PoliMi and the morphing wing scaled model.

The wing model is designed as a modular structure made of aluminum ribs and C shaped front and rear spars, while a transparent polycarbonate skin allow to control the actuation mechanisms inside. The morphing leading and trailing edge are attached to the front and rear spars. Details of the wing box model are shown in Figure 29.

Figure 29 The wind tunnel model wing box with morphing devices.

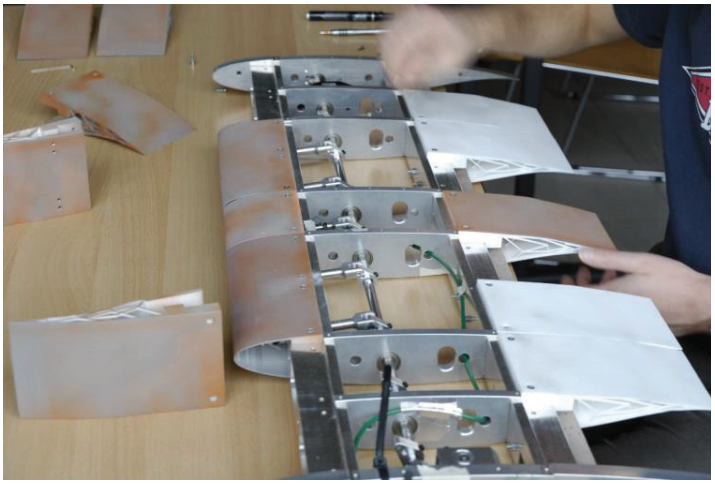

The actuation system is based on the use of off-the-shelf servo actuators used for robotic and aircraft modeler applications. The wing model is connected from the side ribs to an already available rig used for dynamic stall investigation on helicopter blades, allowing for an automatic variation of the angle of attack. The rig includes a load cell to measure the loads acting on the wing model. Figure 29 shows the wing box and the morphing leading and trailing edge devices after they have been assembled.

The manufacturing of the compliant structures on a such as small scale represents a challenge due to the need to exactly reproduce the thickness distribution as well as the need to obtain small thicknesses due to the reduced scale adopted. For this reason, different approaches have been investigated. One of the most promising appears at the moment the one based on the 3D printing technology. This technology is commonly referred with a single word, i.e. 3D printing but it includes many and different additive material techniques, such as for example FDM, SLA, SLS and PolyJet. The first test on FDM technology were not fully satisfactory, due to the low accuracy in the finally obtained thickness distribution. Much better results have been obtained by Stereolithography (SLA) and Sintering (SLS) technologies so that these two techniques has been selected for the morphing device prototypes. Consequently the materials used to manufacture the complete morphing leading and trailing edge are respectively ABS and Nylon. Figure 29 shows the final compliant structures obtained starting from the CAD models of Figure 27. Measurement of the morphing shape was performed outside the wind tunnel before, in separate ground tests. Correctly actuated, they are able to change their shape as shown in Figure 30, where the deformations of the compliant devices, corresponding to downward deflections, are presented for both leading and trailing edge.

Figure 30 Undeformed and deformed compliant leading edge attached to the front spar (left and middle) and deformed compliant trailing edge attached to the rear spar (right).

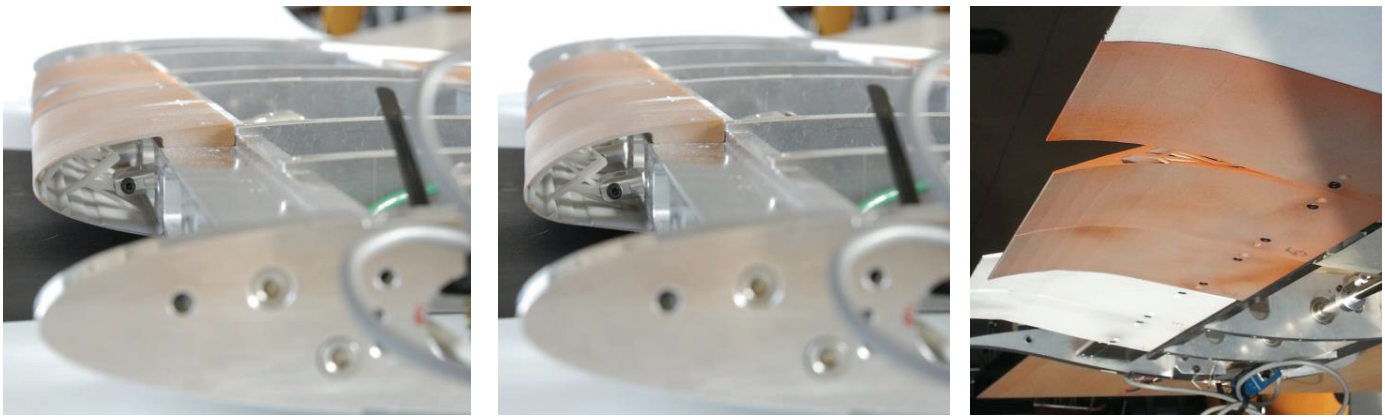

The wind tunnel test matrix involves running four different configurations (undeformed, downward deflection of the morphing leading edge, downward deflection of the morphing trailing edge and the combination of both) at speeds from 20 to 40 m/s at 10 m/s increments and angles of attack from 0° to +10° at 2° increments. The tests was conducted to validate the morphing structure under the aerodynamic loads. The instrumentation used in the testing includes: a) encoder measuring the rotation of the camshaft that control the leading edge actuation; b) 32 pressure tappings at the middle section along the span; c) load cell measuring the actuation force acting on each compliant leading edge rib; d) 1 external camera for photogrammetry. The wind tunnel tests confirmed the functionality of the compliant leading and trailing edge devices under aerodynamic loads and allowed to validate both the codes used during the design process. The pressure

measurements showed a good agreement with the CFD and are used to validate the shape optimization procedure and the aerodynamic results obtained by PHORMA. The leading and trailing surface shapes that the compliant devices assumed during the wind tunnel test was reconstructed by means of a specific full—field photogrammetry technique able to direct capture spatial information about the compliant structure deformations. The same values of actuation required by the FEM to match the target shapes have been applied to the wind tunnel model (10° of motor rotation for the leading edge and 4 mm of sliding for the trailing edge). Corresponding shapes have been captured, working with data and images collected from the digital camera, and compared with the undeformed shapes to obtain the deformation field of the compliant leading and trailing edge. The digitized shapes have been interpolated in order to extract 2D curves corresponding to a wing cross section. The deformed curves shown in Figure 31 have been used to compute the experimental LSE with respect to the target shape of Figure 19. The wind tunnel compliant devices guarantees a LSE values of 2.8e-4 m for the downward deflection of the leading edge and 5.4e-4 m for the downward deflection of the trailing edge that are better than the numerical LSE values obtained from the Pareto Front. This first wind tunnel test allowed to validate the code SPHERA and the “design-through-optimization” procedure adopted by PoliMi for the design of morphing wing devices based on compliant mechanisms.

Figure 31 Digitized shapes corresponding to the downward deformations of the compliant leading and trailing edge, captured during experimental tests by means of photogrammetry techniques.

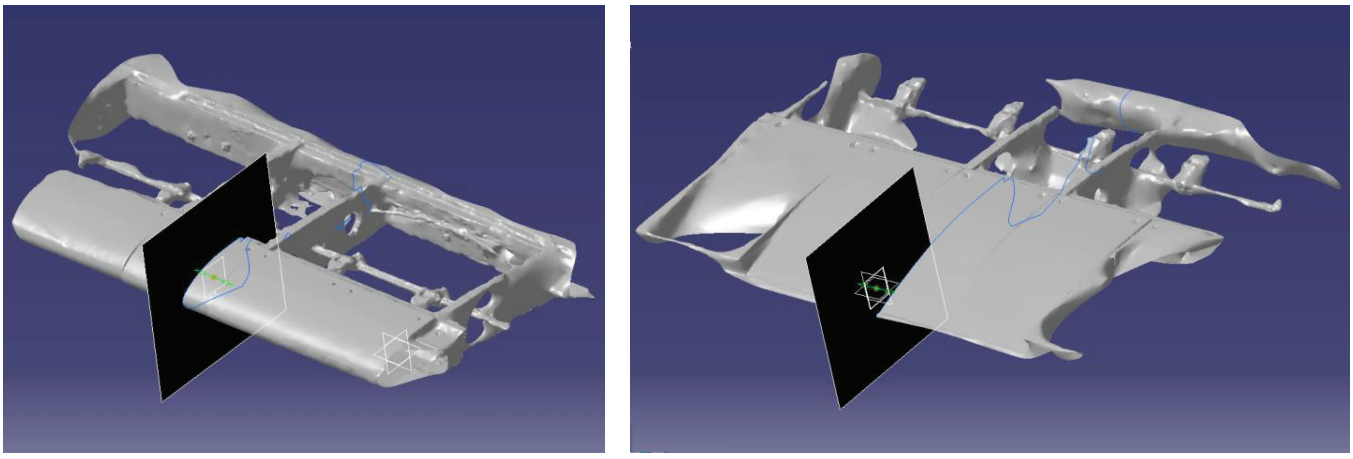

Summary

This paper describes the numerical design tools used for the design of compliant morphing devices for a regional jetliner wing and wingtip. These tools have been shown to be highly useful design aids and manufacturing for preliminary experimental testing of the resulting designs have been presented. The results of the first experimental tests provided insights into the effectiveness of topology optimization methods for the design of morphing structures.

Acknowledgments

The presented work is carried out as part of the EU FP7 Project NOVEMOR and the authors thank the European Commission for funding this research (Grant Agreement 285395). Srinivas Vasista is a recipient of an Alexander von Humboldt Postdoctoral Research Fellowship and is grateful for the financial support from the Alexander von Humboldt Foundation. The authors also gratefully acknowledge Prof. Krister Svanberg for providing the MMA Matlab codes.

References

ACARE (2001), *European Aeronautics: A Vision for 2020*, Advisory Council for Aeronautics Research in Europe.

Barbarino, S. et al. (2011), "A Review of Morphing Aircraft", *Journal of Intelligent Material Systems and Structures*, 22(9), pp.823–877.

Bendsøe, M.P. (1989), "Optimal shape design as a material distribution problem", *Structural Optimization*, 1(4), pp.193–202.

Community Research and Development Service (CORDIS) (2012), *Transport (including Aeronautics)*, Available at: http://cordis.europa.eu/fp7/transport/ [Accessed February 26, 2015].

European Commission (2011), Flightpath 2050: Europe ' s Vision for Aviation, Belgium.

Deb K., Pratap A., Agarwal S. and Meyarivan T. (2002), "A Fast and Elitist Multiobjective Genetic Algorithm: NSGA—II", *IEEE Transactions On Evolutionary Computation*, 6, 182—197.

De Gaspari, A. (2010), "A two levels approach for the optimal design of morphing wings based on compliant structures", Ph.D. Dissertation, Politecnico di Milano, Milano.

De Gaspari, A. and Ricci, S. (2011), "A Two-Level Approach for the Optimal Design of Morphing Wings Based On Compliant Structures", *Journal of Intelligent Material Systems and Structures*, 22(10), pp.1091–1111.

De Gaspari, A. and Ricci, S. (2014), "Application of the Active Camber Morphing Concept Based on Compliant Structures to a Regional Aircraft", *SPIE - Industrial and Commercial Applications of Smart Structures Technologies 2014*, San Diego, CA, USA, 9 March.

Ghiringhelli, G.L., Masarati, P. and Mantegazza, P. (2000), "Multibody implementation of finite volume C0 beams", *AIAA Journal*, 38(1), 131—138.

Kang, Z. & Tong, L. (2007), "Integrated Optimization of Material Layout and Control Voltage for Piezoelectric Laminated Plates", *Journal of Intelligent Material Systems and Structures*, 19(8), pp.889–904.

Kintscher, M. et al. (2011), "Design of a smart leading edge device for low speed wind tunnel tests in the European project SADE", *International Journal of Structural Integrity*, 2(4), pp.383–405.

Kulfan, B.M. (2008), "Universal parametric geometry representation method", *Journal of Aircraft*, 45(1), 142—158.

Lagarias, J.C. et al. (1998), "Convergence Properties of the Nelder--Mead Simplex Method in Low Dimensions", *SIAM Journal on Optimization*, 9(1), pp.112–147.

Lu, K.-J. & Kota, S. (2005), "An Effective Method of Synthesizing Compliant Adaptive Structures using Load Path Representation", *Journal of Intelligent Material Systems and Structures*, 16(4).

Luo, Z. et al. (2011), "Shape morphing of laminated composite structures with photostrictive actuators via topology optimization", *Composite Structures*, 93(2), pp.406–418.

Maute, K. & Reich, G.W. (2006), "Integrated Multidisciplinary Topology Optimization Approach to Adaptive Wing Design", *Journal of Aircraft,* 43(1), pp. 253-263.

Mlejnek, H.P. (1992), "Some aspects of the genesis of structures", *Structural Optimization*, 5(1-2), pp.64–69.

Norris, G. (2015), "FlexSys-Built Morphing Flap Tested To Higher Deflections", *Aviation Week and Space Technology*. Available at: http://aviationweek.com/technology/flexsys-built-morphing-flap-tested-higher-deflections [Accessed February 26, 2015].

Pedersen, C.B.W., Buhl, T. & Sigmund, O. (2001), "Topology synthesis of large-displacement compliant mechanisms", *International Journal for Numerical Methods in Engineering*, 50(12), pp.2683–2705..

Radestock, M. et al. (2014), "Structural Optimization of an UAV Leading Edge with Topology Optimization", *DeMEASS*.

Rudenko, A., Monner, H.P. & Rose, M. (2014), "A Process Chain for Structural Optimization of a Smart Droop Nose for an Active Blown High Lift System", *22nd AIAA/ASME/AHS Adaptive Structures Conference*, pp.1–6.

Santer, M. & Pellegrino, S. (2009), "Topological Optimization of Compliant Adaptive Wing Structure", *AIAA Journal*, 47(3), pp.523–534..

Sofla, A.Y.N. et al. (2010), "Shape morphing of aircraft wing: Status and challenges", *Materials & Design*, 31(3), pp.1284–1292.

Stanewsky, E. (2000), "Aerodynamic benefits of adaptive wing technology", *Aerospace Science and Technology*, 4(7), pp.439–452.

Suleman, A. et al. (2014), "Novel Air Vehicle Configurations: From Fluttering Wings to Morphing Flight", In *World Congress on Computational Mechanics (WCCM XI)*. Barcelona, Spain, pp. 3–4.

Svanberg, K. (2004), "Some Modelling Aspects for the Matlab Implementation of MMA", Available at: https://people.kth.se/~krille/mmamatlab.pdf [Accessed December 1, 2014].

Svanberg, K. (1987), "The method of moving asymptotes—a new method for structural optimization", *International Journal for Numerical Methods in Engineering*, 24(2), pp.359–373.

Thill, C. et al. (2008), "Morphing skins", *Aeronautical Journal*, 112(1129), pp.117–139.

Thuwis, G.A. (2012), "Stiffness and Layout Tailoring of a Morphing High-Lift System with Aeroelastic Loads", PhD Dissertation, TU Delft.

Vasista, S., Tong, L. & Wong, K.C. (2012), "Realization of Morphing Wings: A Multidisciplinary Challenge", *Journal of Aircraft*, 49(1), pp.11–28.

Weisshaar, T. A. (2013), "Morphing Aircraft Systems: Historical Perspectives and Future Challenges", *Journal of Aircraft*, 50(2), pp.337–353.

Zhou, M. & Rozvany, G.I.N. (1991), "The COC algorithm, Part II: Topological, geometrical and generalized shape optimization", *Computer Methods in Applied Mechanics and Engineering*, 89(1-3), pp.309–336.